Available online at www.sciencedirect.com
SCIENCE DIRECT®
ELSEVIER
International Journal of Solids and Structures 43 (2006) 222–253
INTERNATIONAL JOURNAL OF SOLIDS and STRUCTURES
www.elsevier.com/locate/ijsolstr

Reconcile the perfectly elastoplastic model to simulate the cyclic behavior and ratcheting

Chein-Shan Liu *

Department of Mechanical and Mechatronic Engineering, Taiwan Ocean University, Keelung 20224, Taiwan

Received 23 August 2004; received in revised form 21 April 2005
Available online 6 June 2005

Abstract

Perfectly elastoplastic constitutive model is modified through a smoothing factor introduced by Liu [Liu, C.-S., 2003. Smoothing elastoplastic stress–strain curves obtained by a critical modification of conventional models. Int. J. Solids Struct. 40, 2121–2145]. The new model allows plasticity to happen in a non-zero-measure yield volume in stress space, rather than that of conventional zero-measure yield surface, and within the yield volume the plastic modulus is varying continuously. It endows a specific strain-hardening rule of flow stress and is able to describe the phenomena of strain hardening, cyclic hardening, the Bauschinger effect, mean-stress relaxation, strain ratcheting, out-of-phase hardening, as well as erasure-of-memory. In order to suppress the over prediction of ratcheting we consider a scalar function of smoothing factor, which can simulate the saturation behavior of uniaxial/multiaxial strain ratcheting. These effects are demonstrated through numerical examples. The existence of stress equilibrium point and limiting surface is a natural result without requiring an extra design. Moreover, the non-linear constitutive equations can be converted into a linear system for augmented stress in the Minkowski space, of which the symmetry group is a proper orthochronous Lorentz group $SO_o(5,1)$. The augmented stress is a time-like vector, moving on hyperboloids inside the cone. When taking the Prager kinematic hardening rule into account we can simulate some cyclic behaviors of SAE 4340 and grade 60 steels within a certain accuracy through the use of only three material constants and a fixed smoothing factor. To simulate the ratcheting behaviors of SS304 stainless steel we allow the smoothing factor to be an exponential decaying function of λ.

Keywords: Elastoplasticity; Smoothing factor; Cyclic behavior; Strain ratcheting; Minkowski spacetime; Lorentz group

* Tel.: +886 2 2462 2192/3252; fax: +886 2 2462 0836.
E-mail address: csliu@mail.ntou.edu.tw

0020-7683/$ - see front matter © 2005 Elsevier Ltd. All rights reserved.
doi:10.1016/j.ijsolstr.2005.04.019

1. Introduction

For its simplicity without considering the hardening effect and revealing a sharp transition between elastic and plastic phases, the perfectly elastoplastic model is hardly to match the requirements of modeling the cyclic behavior, of which Dafalias (1984) has announced the following five points: (a) unsymmetric stress cycles will cause cyclic creep in the direction of mean stress, (b) unsymmetric strain cycles will cause progressive relaxation to zero mean stress, (c) the model must predict as accurately as possible the variation of plastic modulus during a random cyclic loading, (d) under symmetric stress or strain cycle, the material hardens or softens towards a properly defined stabilized state with only kinematic hardening, and (e) an extensive plastic loading along almost one fixed direction overwhelms and wipes out many of the past history effects, if not all.

Drucker (1988) has classified the elastoplastic constitutive models into two types: conventional and unconventional. The conventional one is based on the assumption that the interior of yield surface is an elastic domain, wherein plastic deformation is not permitted no matter what stress changes occur. Conversely, the unconventional one may allow plasticity to happen inside the yield surface. In order to differentiate these two situations, Hashiguchi (1989) called the plastic state in which stress point lies on the conventional yield surface a "normal-yield state" and the plastic state within the yield surface a "subyield state."

The constitutive model whose interior of the normal-yield surface is assumed to be an elastic region has severe limitations: (a) the discontinuous stress rate and strain rate relation is predicted, which changes abruptly when stress reaches the normal-yield surface; (b) the loading criterion requires the judgement whether the current stress lies on the normal-yield surface or not; (c) upon yielding the consistent condition requires the subsequent stress points being kept on the normal-yield surface; and (d) the hysteresis loop for partial unloading–reloading, the Masing effect and the strain ratcheting phenomenon cannot be described. To remedy, various unconventional constitutive models have been proposed for simulating the cyclic behavior in the past few decades. In contrast to the conventional single yield-surface plasticity theory, Mróz (1967) proposed a multi-surface model with an associated kinematic hardening rule. Thereafter, a simplified two-surface model employing a normal-yield surface and only one subyield surface enclosing a purely elastic domain has been formulated by Dafalias and Popov (1975, 1976), Krieg (1975), Mróz et al. (1979), Tseng and Lee (1983) and Hashiguchi (1988). In the plural surfaces theory, there are also the infinite-surface model developed by Mróz et al. (1981), and the subloading surface model developed by Hashiguchi (1989).

In terms of the mechanical requirements for cyclic plasticity, namely, the conditions of continuity in the large and in the small and the Masing effect, Hashiguchi (1993) has examined those models in detail. One of these requirements needs the material model to respond plastically under a loading process even starting immediately from a zero stress state. That is, the elastic domain is shrunk to a stress point under the loading condition, which is however not true for most metals which being loaded from their annealed states. As remarked by Hashiguchi (1993) only a very few models can meet these stringent requirements.

In the present paper we revisit the conventional perfectly elastoplastic model, and propose a simple but critical modification such that some improvements on the modeling of cyclic behavior can be achieved. These results are however impossible for the original perfectly elastoplastic model. Although our modification is limited to perfectly elastoplastic model, this technique of modification is considered important in plasticity theory, when more complicated yield-surfaces and hardening mechanisms are used in the material modeling.

The elastoplasticity of solid materials proposed by Prandtl (1924) and Reuss (1930) is formulated as the following constitutive differential equation with switching criteria (e.g., Hong and Liu, 1997; Liu and Hong, 2000):

$$\dot{\mathbf{s}} + \frac{\dot{\lambda}}{\gamma_y}\mathbf{s} = 2G\dot{\mathbf{e}}, \tag{1}$$

where the plastic multiplier $\dot{\lambda}$ is subjected to

$$\dot{\lambda} = \frac{1}{\tau_y^0}\mathbf{s}\cdot\dot{\mathbf{e}} > 0 \quad \text{if } \|\mathbf{s}\| = \sqrt{2}\tau_y^0 \text{ and } \mathbf{s}\cdot\dot{\mathbf{e}} > 0, \tag{2}$$

$$\dot{\lambda} = 0 \quad \text{if } \|\mathbf{s}\| < \sqrt{2}\tau_y^0 \text{ or } \mathbf{s}\cdot\dot{\mathbf{e}} \leqslant 0, \tag{3}$$

and

$$\gamma_y := \frac{\tau_y^0}{G} \tag{4}$$

is the shear yield strain with $G > 0$ and $\tau_y^0 > 0$, respectively the shear modulus and the shear yield strength.

Here, $\|\mathbf{s}\| = \sqrt{2}\tau_y^0$ is called the yield condition as shown in Fig. 1(a), which displays schematically the set of all allowable stress states as a closed ball in the stress space of $\mathbf{s}$, consisting of an open ball of elastic states and its boundary, a hypersphere with plastic irreversibility. $\|\mathbf{s}\| := \sqrt{\mathbf{s}\cdot\mathbf{s}}$ denotes the Euclidean norm of $\mathbf{s}$, and a dot between two tensors represents their inner product. The bold-faced $\mathbf{e}$ and $\mathbf{s}$ are, respectively, the deviatoric tensors of strain and stress, both symmetric and traceless, whereas λ is a scalar.

From above it is clear that $\dot{\lambda}$ usually jumps from a zero value in the elastic phase to a finite value in the plastic phase determined by $\mathbf{s}\cdot\dot{\mathbf{e}}/\tau_y^0$. This fact indeed makes the stress–strain curve integrated from Eq. (1) with a discontinuous $\dot{\lambda}$ non-smooth. Unless $\mathbf{s}\cdot\dot{\mathbf{e}} = 0$ at the elastoplastic transition point, the stress–strain curve obtained is usually not of $\mathbb{C}^1$ type. In Section 2 we would show its shortcomings in the modeling of cyclic behavior, and propose a newly modified model, whose resulting stress–strain curves are gradually becoming the $\mathbb{C}^1$ type almost.

Rather early, Masing (1926) proposed a hypothesis for one-dimensional hysteretic behavior of materials by thinking it as consisting of a collection of many perfectly elastoplastic elements, all of which have the same elastic stiffness but with different yield stress levels. Later, Whiteman (1959), based on the same idea, derived a uniaxial stress–strain relation of such a model by introducing the concept of distribution function for the yield stress levels of perfectly elastoplastic elements. Then, Iwan (1966, 1967), who referred to such models as the Distributed-Element-Models (DEMs), applied them to the structural dynamics and extended them into multi-dimensional models. In a series of papers, Chiang and Beck (1994), Chiang (1997) and Chiang et al. (2002) have given a thorough study of the related properties of DEMs and indicated that those models have a reasonable prediction capability of metals behavior under complicated multiaxial cyclic loading conditions. However, the numerical implementation of such a class of multi-dimensional DEMs or their finitely-discretized-elements version involving the calculations of many elements' response and their superposition, is quite difficult and computationally inefficient. Recently, Ramrakhyani et al. (2004) have extended the same idea together with the fractional derivative technique to the modeling of elastomeric materials.

Even, it is possible to use the multi-surface models to simulate the gradual yielding behavior of materials, and various multi-surface models have shown their effectiveness and capability in modeling the plastic

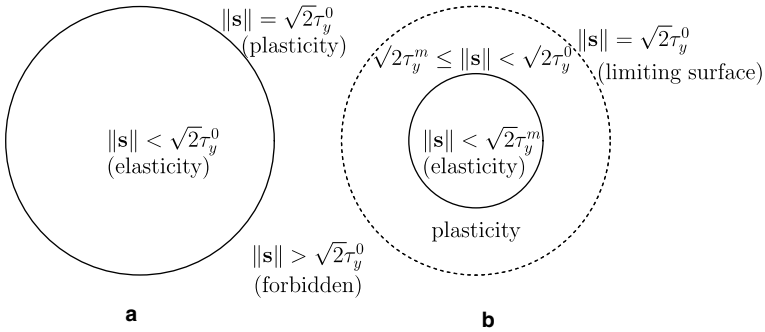

Fig. 1. Allowable stress regions for (a) perfect elastoplasticity and (b) modified perfect elastoplasticity.

behavior under both monotonic and cyclic loading conditions, in this paper we begin with a simple model of perfect elastoplasticity and propose a modification by introducing a smoothing factor in Section 2, where a geometric demonstration is presented. After that, in Section 3 the understanding of the new model behavior may be achieved through the investigations in terms of equilibrium stress point, limiting surface, smooth yielding, strain hardening, the Bauschinger effect, cyclic hardening, the erasure of memory, mean-stress relaxation, strain ratcheting and the continuity of plastic modulus. We point out that the yield surface in stress space for the conventional plasticity theory is really the source of the non-smoothness of its stress–strain curves. Remarkably, a simple modification to be done here makes a big improvement of the simulation capability of cyclic behavior. What might be more interesting is that the new model provides a mathematical tool for understanding the mechanisms in cyclic plasticity. Some comparisons with the two-surface model, the infinite-surface model and the subloading surface model are also made. Then, in Section 4 we convert the non-linear constitutive equations of the new model into an augmented linear system. The mathematical natures including the underlying space of the new model, the Lie algebra, symmetry group and hardening mechanism are explored. For the computational purpose we also develop a group-preserving scheme. Finally, we compare the theoretical results of the new model equipped with the Prager kinematic hardening rule with some experimental data and draw some conclusions in Sections 5 and 6, respectively.

2. A modification of perfectly elastoplastic model

The model of plasticity is known as rate independent. The stress response depends on strain path but is independent of strain rate. Consider two rectilinear strain paths both starting from a point $\mathbf{e}_1$ and ending at another point $\mathbf{e}_2$ in strain space, one with rate $\mathrm{d}\mathbf{e}(t)/\mathrm{d}t$ and the other one with rate $\mathrm{d}\mathbf{e}(t')/\mathrm{d}t'$, where t and t' have a monotonic relation, i.e., $\mathrm{d}t'/\mathrm{d}t > 0$. Multiplying Eqs. (1)–(3) by $\mathrm{d}t/\mathrm{d}t'$ we get the same equations but with a dependence on t merely replaced by a dependence on t' of $\mathbf{e}$, $\mathbf{s}$ and λ. The response $\mathbf{s}_2$ at the strain point $\mathbf{e}_2$ are the same if in that two parameterizations the stresses have the same initial point $\mathbf{s}_1$. Therefore, both t and t' can be equally the independent variable of plasticity equations, and it makes no distinction between the use of t or t'. However, for convenience, the independent variable no matter what it is will be simply called "time" and given the symbol t.

In order to focus on the study of fundamental plasticity behavior we begin with perfectly plastic model which, displaying no any hardening effect, is amenable to a modification showing a visible improvement to reveal different hardening mechanisms in the course of cyclic loadings. The conventional kinematic hardening rule due to Prager (1956) accounting of the deformation induced directional anisotropy is not required here until Section 5, where we combine it with the modified model to simulate some experimental results reported in the literature. On the other hand, in order to get a better description of the material cyclic hardening/softening behavior we need to consider a modification of the isotropic hardening/softening model as that given by Liu (2003).

2.1. The motivation

A rectilinear strain path is specified by a given second-order constant deviatoric tensor $\mathbf{c}$:

$$\mathbf{e}(t) = \mathbf{e}(t_i) + \mathbf{c}(t - t_i) \tag{5}$$

during a time interval of $t \geqslant t_i$.

Referring to Fig. 2, the distance from an admissible stress $\mathbf{s}(t_{\mathrm{off}})$ at time $t = t_{\mathrm{off}}$[1] to the yield surface along the direction $\mathbf{c}$ is denoted by $\|\Delta\mathbf{s}\|$, which can be proved to be

[1] t_{off} may be any time of an elastic phase or a time for the occurrence of a reverse unloading. Admissible stress for the perfectly elastoplastic model is $\|\mathbf{s}\| \leqslant \sqrt{2}\tau_y^0$ as shown in Fig. 1(a).

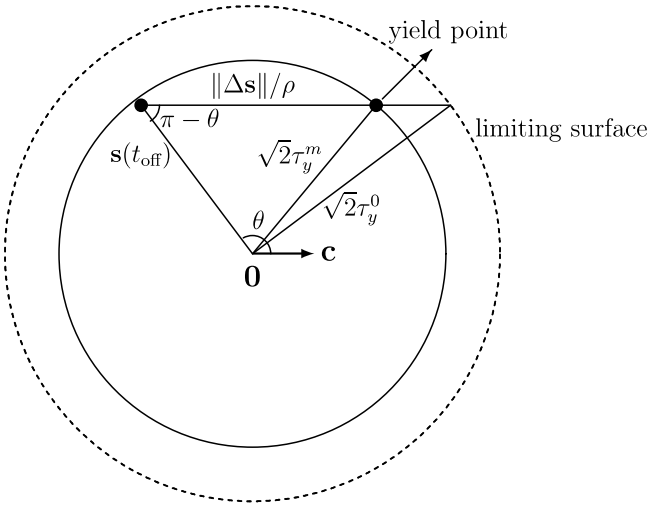

Fig. 2. A geometric construction of the modified shear yield stress τ_y^m. θ is the angle between $\mathbf{s}(t_{\text{off}})$ and $\mathbf{c}$.

$$\begin{aligned}\|\Delta\mathbf{s}\| &= \sqrt{2(\tau_y^0)^2 - [\|\mathbf{s}(t_{\text{off}})\|\sin(\pi-\theta)]^2} + \|\mathbf{s}(t_{\text{off}})\|\cos(\pi-\theta)\\ &= \sqrt{2(\tau_y^0)^2 - \|\mathbf{s}(t_{\text{off}})\|^2\sin^2\theta} - \|\mathbf{s}(t_{\text{off}})\|\cos\theta,\end{aligned} \tag{6}$$

where θ is the angle between $\mathbf{s}(t_{\text{off}})$ and $\mathbf{c}$. For the perfectly elastoplastic model the stress path starting from a reference state $\mathbf{s}(t_{\text{off}})$ needs to trace a distance $\|\Delta\mathbf{s}\|$ to begin the yielding state. Dividing the above $\|\Delta\mathbf{s}\|$ by the stressing speed $2G\|\mathbf{c}\|$ we obtain an elapsed time $t_{\text{on}} - t_{\text{off}}$ as shown by

$$t_{\text{on}} = t_{\text{off}} + \frac{\sqrt{2(\tau_y^0)^2 - \|\mathbf{s}(t_{\text{off}})\|^2\sin^2\theta} - \|\mathbf{s}(t_{\text{off}})\|\cos\theta}{2G\|\mathbf{c}\|}. \tag{7}$$

Integrating Eq. (1) with $\dot{\lambda} = 0$ from t_{off} to t gives an elastic response:

$$\mathbf{s}(t) = \mathbf{s}(t_{\text{off}}) + 2G(t - t_{\text{off}})\mathbf{c}. \tag{8}$$

Simultaneously, under the strain path (5) the plastic response can be derived in a closed-form (Hong and Liu, 1998):

$$\mathbf{s}(t) = \frac{\mathbf{s}(t_{\text{on}}) + \{C_1[\mathrm{e}^{m(t-t_{\text{on}})} - 1] + C_2[1 - \mathrm{e}^{-m(t-t_{\text{on}})}]\}\bar{\mathbf{c}}}{C_1\mathrm{e}^{m(t-t_{\text{on}})} + C_2\mathrm{e}^{-m(t-t_{\text{on}})}}, \tag{9}$$

where

$$m := \frac{\sqrt{2}\|\mathbf{c}\|}{\gamma_y}, \quad \bar{\mathbf{c}} := \frac{2G\mathbf{c}}{m} = \frac{\sqrt{2}\tau_y^0\mathbf{c}}{\|\mathbf{c}\|}, \tag{10}$$

$$C_1 := \frac{1}{2}\left[1 + \frac{\mathbf{s}(t_{\text{on}})\cdot\mathbf{c}}{m\gamma_y\tau_y^0}\right], \quad C_2 := \frac{1}{2}\left[1 - \frac{\mathbf{s}(t_{\text{on}})\cdot\mathbf{c}}{m\gamma_y\tau_y^0}\right]. \tag{11}$$

Although the behavior of perfectly elastoplastic model under rectilinear strain paths has been studied thoroughly by Hong and Liu (1998), we show three uniaxial cyclic stress–strain curves in Fig. 3 to disclose its shortcomings. In all calculations G is fixed to be 20,000 MPa and τ_y^0 to be 200 MPa. The calculations

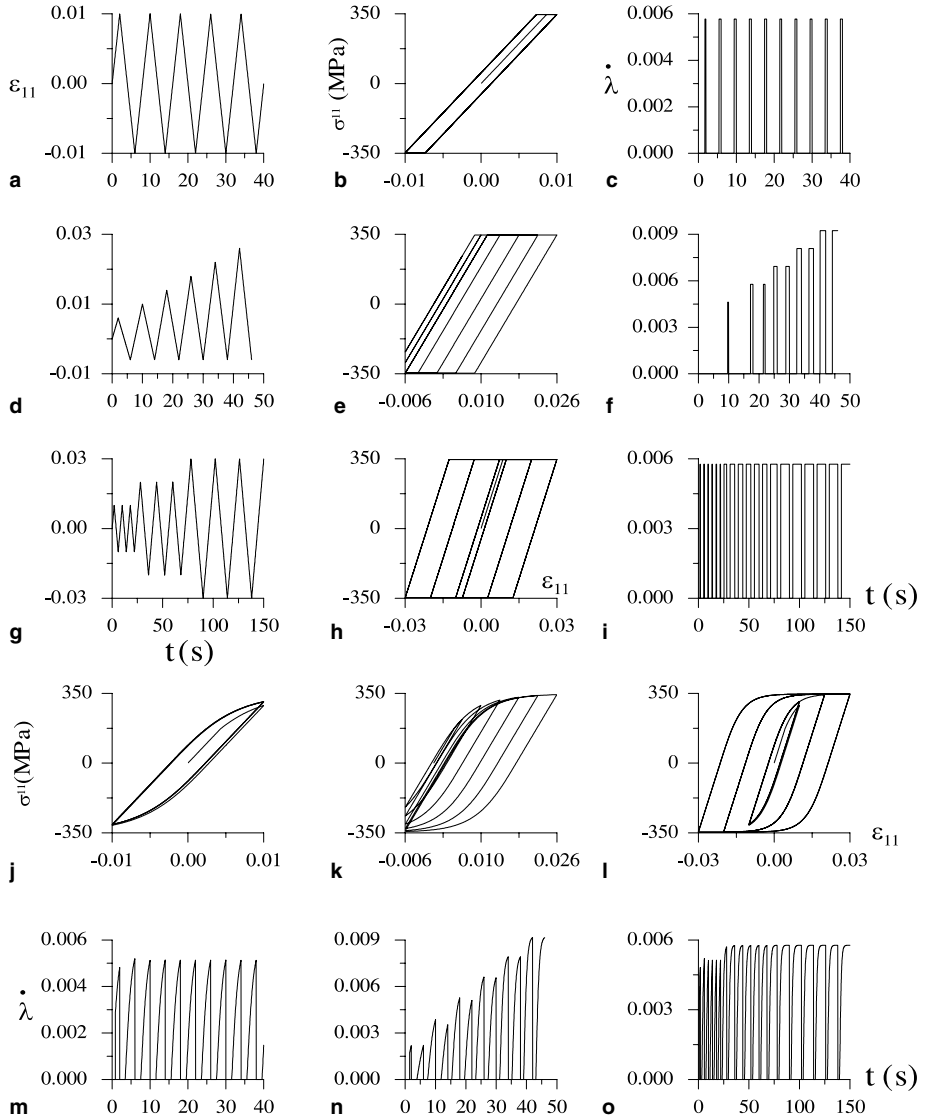

Fig. 3. The uniaxial behavior of the perfectly elastoplastic model: (a) the time history of axial strain with constant strain amplitude, (b) the response curve of axial stress, (c) the time history of the plastic multiplier; the results for cyclically increasing strain amplitude in positive direction are shown in (d)–(f), and the results for piecewise increasing strain amplitude are shown in (g)–(i). The uniaxial behavior of the new model under the same strain inputs: (j)–(l) are the response curves of axial stress, and (m)–(o) are the time histories of the plastic multiplier.

were based on Eq. (8) for the elastic phase and Eq. (9) for the plastic phase. However, since the strain paths we use are piecewise rectilinear, and the formulae are suitable for each single rectilinear strain path with a specified initial stress, in a practical numerical computation the global solution is obtained by piecing together the solutions of the consecutive pieces.

Fig. 3(a)–(c) shows, respectively, the time history of axial strain ε_{11} with constant strain amplitude, the response curve of axial stress σ^{11} and the time history of $\dot{\lambda}$. The results for a cyclically increasing strain

amplitude in the positive direction are shown in Fig. 3(d)–(f), and the results for piecewisely increasing strain amplitude are shown in Fig. 3(g)–(i). Obviously, all these stress–strain curves are too over-square at the elastoplastic transition points, and none of them can properly reflect the real behavior of metals. The corresponding time histories of $\dot{\lambda}$ are shown, respectively, in Fig. 3(c), (f) and (i); clearly, the jump of $\dot{\lambda}$ from zero value to finite value is the main reason to cause the non-smoothness of each stress–strain curve.

2.2. A new model

In order to overcome the above shortcomings of non-smoothness and over-squareness of response curves and to reconcile the perfectly elastoplastic model to a new one which able to simulate the cyclic behavior, instead of the constant shear yield stress τ_y^0 we propose a modified shear yield stress τ_y^m, such that $\dot{\lambda}$ in Eq. (1) is modified by subjecting to the new switching criteria:

$$\dot{\lambda} = \frac{1}{\tau_y^0}\mathbf{s}\cdot\dot{\mathbf{e}} > 0 \quad \text{if } \sqrt{2}\tau_y^0 > \|\mathbf{s}\| \geqslant \sqrt{2}\tau_y^m \text{ and } \mathbf{s}\cdot\dot{\mathbf{e}} > 0, \tag{12}$$

$$\dot{\lambda} = 0 \quad \text{if } \|\mathbf{s}\| < \sqrt{2}\tau_y^m \text{ or } \mathbf{s}\cdot\dot{\mathbf{e}} \leqslant 0. \tag{13}$$

For the original perfectly elastoplastic model if its stress path starts from a reference state $\mathbf{s}(t_{\text{off}})$ it needs to trace a distance $\|\Delta\mathbf{s}\|$ as given by Eq. (6) to start a yielding; however, for the new model we suppose that it starts to yield by tracing forward a much shorter distance of $\|\Delta\mathbf{s}\|/\rho$ with $\rho > 1$. Hence, referring to Fig. 2 again we obtain

$$\begin{aligned} 2(\tau_y^m)^2 &= [\|\mathbf{s}(t_{\text{off}})\|\sin(\pi-\theta)]^2 + \left[\frac{\|\Delta\mathbf{s}\|}{\rho} - \|\mathbf{s}(t_{\text{off}})\|\cos(\pi-\theta)\right]^2 \\ &= \|\mathbf{s}(t_{\text{off}})\|^2\sin^2\theta + \frac{1}{\rho^2}\left[(\rho-1)\|\mathbf{s}(t_{\text{off}})\|\cos\theta + \sqrt{2(\tau_y^0)^2 - \|\mathbf{s}(t_{\text{off}})\|^2\sin^2\theta}\right]^2, \end{aligned} \tag{14}$$

where $\|\Delta\mathbf{s}\|$ defined by Eq. (6) was inserted into the first equality to derive the second equality. The above t_{off} is the latest unloading time, or any time of an elastic state with a given $\mathbf{s}(t_{\text{off}})$. $\rho > 1$ is a smoothing factor determined by experimental test; when $\rho = 1$, $\tau_y^m = \tau_y^0$, and we return to the original perfectly elastoplastic model.

Hereafter, we call the perfectly elastoplastic model with the above modification the *new model*, and which without considering the above modification the *original model*. In the new model we really depress the original shear yield strength level τ_y^0 to a lower level τ_y^m, and when $\|\mathbf{s}\| \geqslant \sqrt{2}\tau_y^m$ we call the material yielding. It allows plasticity occurring within a finite stress volume in $\sqrt{2}\tau_y^0 > \|\mathbf{s}\| \geqslant \sqrt{2}\tau_y^m$ as schematically shown in Fig. 1(b). The original yield surface $\|\mathbf{s}\| = \sqrt{2}\tau_y^0$ must be viewed as a limiting surface in the new theory; see the discussions below.

Because the original model and the new model possess the same governing Eq. (1) and the same $\dot{\lambda} = \mathbf{s}\cdot\dot{\mathbf{e}}/\tau_y^0$, Eq. (9) with the new t_{on} (derived in Appendix A):

$$t_{\text{on}} = t_{\text{off}} + \frac{\sqrt{2(\tau_y^0)^2 - \|\mathbf{s}(t_{\text{off}})\|^2\sin^2\theta} - \|\mathbf{s}(t_{\text{off}})\|\cos\theta}{2\rho G\|\mathbf{c}\|} \tag{15}$$

is still applicable to the new model when it is subjected to the strain path (5); however, the initial stress $\mathbf{s}(t_{\text{on}})$ does not necessarily locate on the yield surface. Indeed we allow $\|\mathbf{s}(t_{\text{on}})\| = \sqrt{2}\tau_y^m < \sqrt{2}\tau_y^0$ for the new model.[2] Accordingly, we can use these equations to calculate the responses of the new model by merely shortening the original switch-on time with a factor ρ.

[2] The admissible stress for the new model is $\|\mathbf{s}\| < \sqrt{2}\tau_y^0$.

3. Character and comments of the new model

3.1. Characterizing the new model behavior

In the cyclic plasticity theory, various phenomena of material behavior have been characterized in order to facilitate our description of stress–strain curves under different loading conditions. A theoretical model is performing well if it is able to reproduce all these phenomena of cyclic plasticity. Based on the new model we are able to elucidate experimentally observed phenomena and effects through some illustrative calculation examples.

3.2. Equilibrium stress point

It is a stress state associated with a unidirectional strain increment at which stress increment approaches zero. The existence of equilibrium stress point for a material in its plastic state is suggested by Lamba and Sidebottom (1978). Below we prove that the new model exists an equilibrium stress point corresponding to each unidirectional strain path as specified by Eq. (5).

By letting $t \to \infty$ in Eq. (9), it follows that

$$\lim_{t\to\infty} \mathbf{s}(t) = \bar{\mathbf{c}}. \tag{16}$$

Moreover, by means of Eqs. (12), (5) and (16) we obtain

$$\lim_{t\to\infty} \dot{\lambda} = \frac{1}{\tau_y^0} \lim_{t\to\infty} \mathbf{s}\cdot\mathbf{c} = \sqrt{2}\|\mathbf{c}\|. \tag{17}$$

Taking the limit in both the sides of Eq. (1) and substituting Eqs. (16) and (17) into the resultant lead to

$$\lim_{t\to\infty} \dot{\mathbf{s}}(t) = 2G \lim_{t\to\infty} \left[\dot{\mathbf{e}}(t) - \frac{1}{2\tau_y^0}\dot{\lambda}(t)\mathbf{s}(t)\right] = \mathbf{0}. \tag{18}$$

Obviously, $\bar{\mathbf{c}}$ is an equilibrium stress point.

For the new model subject to the strain path (5), the equilibrium stress point $\bar{\mathbf{c}}$ is asymptotic stable and all the orbits in stress space approach to it. We first substitute Eq. (12) for $\dot{\lambda}$ and the differential of Eq. (5) for $\dot{\mathbf{e}}$ into the inner product of $\mathbf{s}$ with Eq. (1) to obtain

$$\frac{\mathrm{d}\|\mathbf{s}\|^2}{\mathrm{d}t} = 4G\mathbf{s}\cdot\mathbf{c}\left(1 - \frac{\|\mathbf{s}\|^2}{2(\tau_y^0)^2}\right). \tag{19}$$

Under the strain path (5) the new model responds always in the plastic phase once the yielding occurs, and hence $\mathbf{s}\cdot\mathbf{c} > 0$ holds for all $t > t_{\mathrm{on}}$. For any admissible initial stress with $\|\mathbf{s}(t_{\mathrm{on}})\|^2 < 2(\tau_y^0)^2$ and under the condition of $\mathbf{s}\cdot\mathbf{c} > 0$ it is obvious that $\|\mathbf{s}(t)\|^2$ gradually increases with time t; however, when $\|\mathbf{s}(t)\|^2$ is very close to the value of $2(\tau_y^0)^2$, the increasing rate of $\|\mathbf{s}(t)\|^2$ tends to zero, and hence $\mathbf{s}(t)$ approaches to the stress equilibrium point $\bar{\mathbf{c}}$ asymptotically.

3.2.1. Limiting surface

It has been experimentally observed that for the cyclically stabilized materials, the stress state can never go beyond a region bounded by a limiting surface in the corresponding stress space. For demonstrating this concept, let us substitute Eq. (12) for $\dot{\lambda}$ into Eq. (1),

$$\dot{\mathbf{s}} + \frac{\mathbf{s}\cdot\dot{\mathbf{e}}}{\gamma_y\tau_y^0}\mathbf{s} = 2G\dot{\mathbf{e}}, \tag{20}$$

the inner product of which with $\mathbf{s}$ leads to

$$\frac{\mathrm{d}\|\mathbf{s}\|^2}{\mathrm{d}t} = 4G\mathbf{s}\cdot\dot{\mathbf{e}}\left(1-\frac{\|\mathbf{s}\|^2}{2(\tau_y^0)^2}\right). \tag{21}$$

A set $\mathscr{S}$ in $\mathbb{R}^5$ is said to be an *invariant set* of Eq. (20) if, for any point $\mathbf{p}\in\mathscr{S}$ the solution curve through $\mathbf{p}$ belongs to $\mathscr{S}$ for $t\in(-\infty,\infty)$; see, e.g., Hale (1969). In view of Eq. (21) it is obvious that $\mathscr{S} := \{\mathbf{s} \mid \|\mathbf{s}\| = \sqrt{2}\tau_y^0\}$ is an invariant set of Eq. (20). If the initial condition is $\|\mathbf{s}(t_i)\| < \sqrt{2}\tau_y^0$, it is always $\|\mathbf{s}(t)\| < \sqrt{2}\tau_y^0$ for all $t > t_i$. However, for the initial condition of $\|\mathbf{s}(t_i)\| = \sqrt{2}\tau_y^0$, $\|\mathbf{s}(t)\| = \sqrt{2}\tau_y^0$ remains true for all $t > t_i$; and for the initial condition of $\|\mathbf{s}(t_i)\| > \sqrt{2}\tau_y^0$, it is always $\|\mathbf{s}(t)\| > \sqrt{2}\tau_y^0$ for all $t > t_i$. Thus, the three sets of $\|\mathbf{s}(t)\| < \sqrt{2}\tau_y^0$, $\|\mathbf{s}(t)\| = \sqrt{2}\tau_y^0$ and $\|\mathbf{s}(t)\| > \sqrt{2}\tau_y^0$ are disconnected. However, the stress states of the last two cases are excluded by the new model. The state $\|\mathbf{s}(t)\| = \sqrt{2}\tau_y^0$ is the ω-limit set for arbitrary initial conditions under the condition of $\mathbf{s}\cdot\dot{\mathbf{e}} > 0$, and the α-limit set for arbitrary initial conditions under the condition of $\mathbf{s}\cdot\dot{\mathbf{e}} < 0$. This invariant set together with the differential Eq. (20) really characterizes the global property of the new model.

According to the above discussions, the limiting surface is simply the set of all equilibrium stress points, each of which corresponds to a unidirectional strain path. Even $\|\mathbf{s}\| = \sqrt{2}\tau_y^0$ is called the yield surface in the original plasticity theory; however, it should be deemed as a limiting surface in the new plasticity theory. Here, we allow plasticity to happen in a non-zero-measure volume characterized by $\sqrt{2}\tau_y^0 > \|\mathbf{s}\| \geqslant \sqrt{2}\tau_y^m$ in stress space, rather than the usual zero-measure surface $\|\mathbf{s}\| = \sqrt{2}\tau_y^0$ for the original plasticity theory.

Previously, it was shown by Chiang and Beck (1994) and Hong and Liu (1998) that there exists an equilibrium stress point corresponding to each unidirectional strain path for the behavior of perfectly elastoplastic material, and by Chiang and Beck (1994) for the behavior of DEM. The conditions for the existence of limit points have also been studied by Ottosen and Ristinmaa (1996) for the corner plasticity. For the von Mises type mixed-hardening model, Liu (2004) also proved the asymptotic stability of limit point by the Lyapunov's direct method. For its importance, Chiang (1998) has demonstrated that the property of the existence of limit points may be viewed as a necessary condition for any model in cyclic plasticity to exhibit physically consistent and cyclically stabilized behavior.

Now, we are in a good position to explore the concept of limiting surface and concentric yield surfaces by considering a two-dimensional deviatoric problem under the deviatoric square strain path as shown in Fig. 4(a), which starts from point a and ends at point e = a again after one cycle. Under this path the deviatoric stress path is plotted in Fig. 4(b) and there have one limiting surface, and four yield points as remarked by 1, 2, 3, 4 located in four different concentric yield surfaces with four different radii of τ_y^m determined by Eq. (14). When the strain path traces along the first segement $\underline{ab}$, the stress path starts from an elastic phase in the segement $\underline{a1}$, and then makes an excursion on the plastic phase in the segement $\underline{1b}$. When the strain path turns to the second segement $\underline{bc}$, there first occurs an unloading and continues to be in the elastic phase in the segement $\underline{b2}$, and then in the segement $\underline{2c}$ the material is switched-on to a plastic phase. When the strain path turns to the third segement $\underline{cd}$, there first occurs an unloading such that in the segement $\underline{c3}$ the material is in the elastic phase, and then in the segement $\underline{3d}$ the material is in the plastic phase. When the strain path turns to the fourth segement $\underline{de}$, there first occurs an unloading such that in the segement $\underline{d4}$ the material is in the elastic phase, and then in the segement $\underline{4e}$ the material is in the plastic phase. The stress path is located in the region within the limiting surface, and may approach to the limiting surface, for example, the path $\underline{2c}$.

3.2.2. Smooth yielding

For most metals the transition from an elastic state to a plastic state is gradual, due to successive yielding of the individual crystal grain. When $\rho = 1$ it leads to a stress–strain curve that a flat yield line follows an inclined line. In the range of $1 < \rho \leqslant 2$, a larger ρ leads to a more smooth elastoplastic transition and

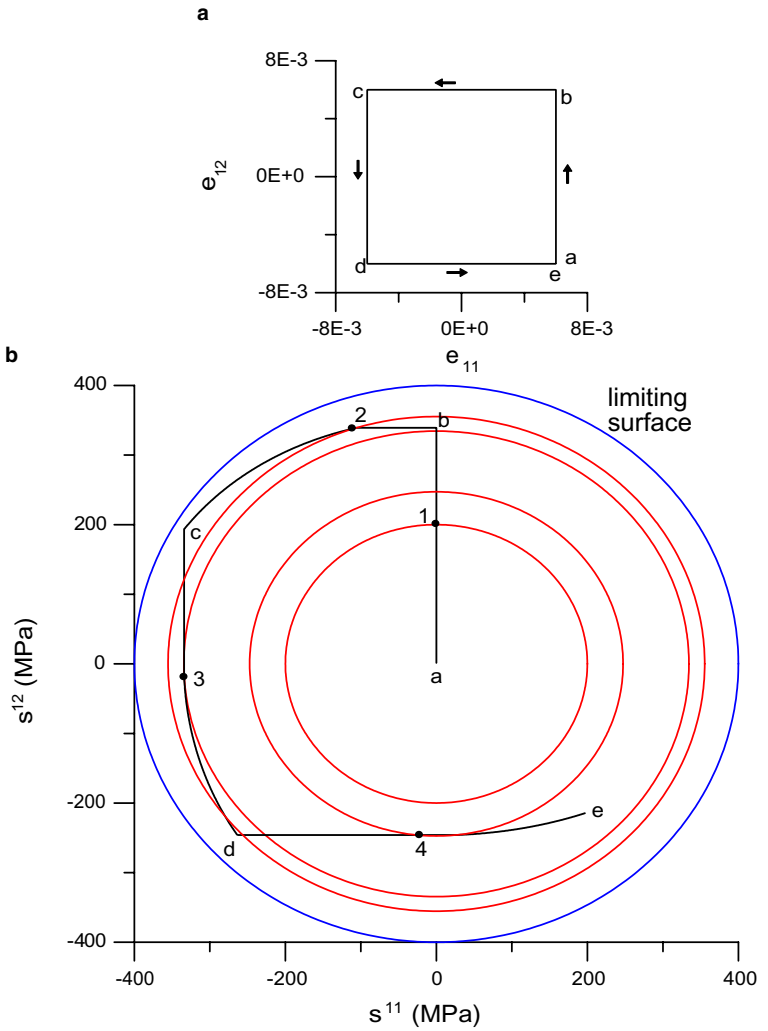

Fig. 4. Under square strain path in (a) the corresponding stress path of the new model is shown in (b).

a larger strain hardening. Now we return to Fig. 3(j)–(o) again, which show the responses of the new model under the same strain inputs as that given, respectively, in Fig. 3(a), (d) and (g). Through this modification it can be appreciated that $\dot{\lambda}$ is varying smoothly from the zero value in elastic phase to the positive value in plastic phase as shown, respectively, in Fig. 3(m)–(o). The corresponding stress–strain curves as shown, respectively, in Fig. 3(j)–(l) reveal that the transitions from elasticity to plasticity are smooth. Fig. 5(a) displays a stress–strain curve of the new model under the strain cycles with increasing amplitude, where $\tau_y^0 = 400$ MPa and $\rho = 2$ were used. For a demonstration, the time history of the modified shear yield strength τ_y^m is also plotted in Fig. 5(b). It can be seen that τ_y^m almost tends to zero value after the first few cycles. This largely depresses the amplitude of stress required to a further plastic deformation, makes $\dot{\lambda} = \mathbf{s} \cdot \dot{\mathbf{e}}/\tau_y^0$ very small at the elastoplastic transition points, and hence renders the stress–strain curve almost being $\mathbb{C}^1$ smooth. Thus, the above mentioned micro-structural yielding behavior is properly reflected by the new model.

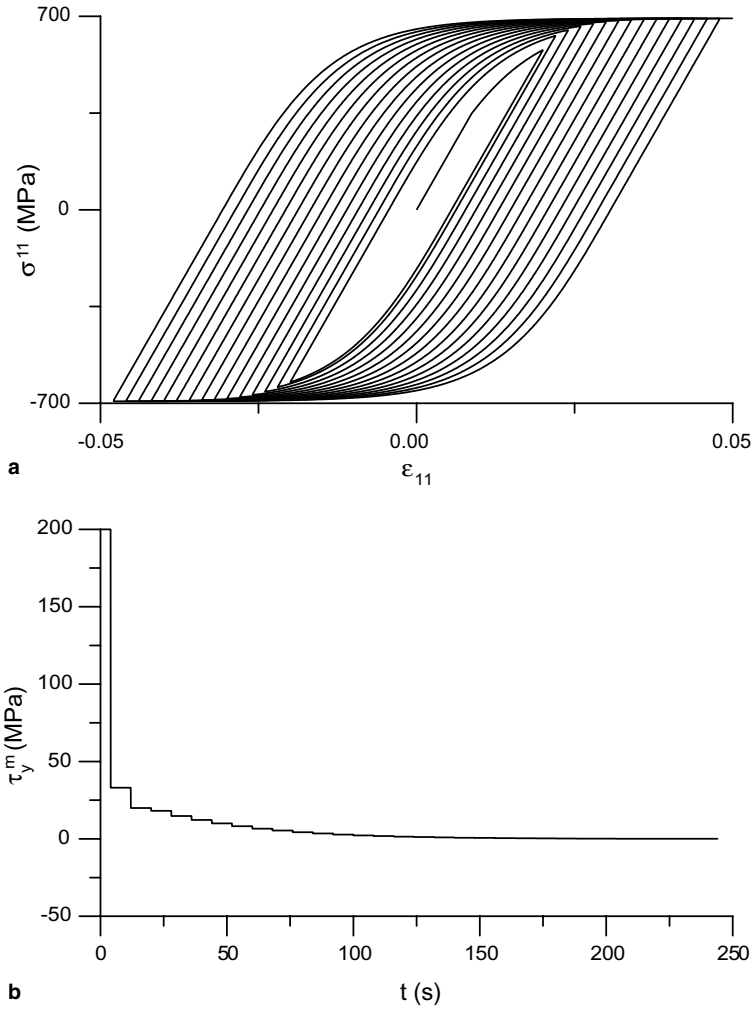

Fig. 5. The uniaxial behavior of the new model under cyclically increasing strain amplitude: (a) the response curve of axial stress and (b) the time history of modified shear yield stress.

3.2.3. Strain hardening[3]

Beyond the yield point, stress continually increases with further plastic strain, while the slope of stress–strain curve, representing the rate of strain hardening, steadily decreases with increasing stress. While the stress–strain curve corresponding to $\rho = 1$ for the original model gives no strain hardening, the new model gives a larger strain hardening for a larger ρ in the range of $1 < \rho \leqslant 2$, and when strain increases the strain hardening rate steadily decreases and each stress–strain curve tends to its limiting stress τ_y^0 (Liu, 2003). Within the context of the new model, the strain hardening comes from the difference between the initial shear yield strength characterized by τ_y^0/ρ and the limiting shear strength characterized by τ_y^0, and also the existence of a limiting surface as discussed above.

[3] In Section 4 we will prove that the new model has a natural strain-hardening law as shown in Eq. (45).

3.2.4. The Bauschinger effect

The yield stress of a specimen in one direction is appreciably smaller in magnitude than that in the opposite direction along which the specimen was loaded. This well-known Bauschinger effect occurs in real metals whenever there is a reversal of stress. In Fig. 6, we compare the one-cycle stress–strain curves for the original model and the new model, where $\tau_y^0 = 300$ MPa and $\rho = 1.5$ were used. Both curves yield initially at the same stress about 346.4 MPa; however, as expected the Bauschinger effect does not appear for the original model, but for the new model the reverse yielding occurs at about -163.3 MPa, whose magnitude is far less than 346.4 MPa, and exhibits the Bauschinger effect.[4]

3.2.5. Cyclic hardening

It is experimentally observed that the hysteresis loop stabilizes after a few cycles of loading. The saturation stress depends on strain amplitude. If the strain amplitude is increased after the stabilization is achieved, the material shows a further hardening until a new stabilization takes place with an increased saturation stress. Such effect on materials is usually called the cyclic hardening (Haupt and Kamlah, 1995; Ristinmaa, 1995).

For the original model no cyclic hardening can be seen in its stress–strain curves as shown in Figs. 3(b), (e), (h) and 6 for different cyclic loading conditions. However, the stress–strain curve of the new model hardens from about 484.4 MPa to about 504.8 MPa after one cycle as shown in Fig. 6. The cyclic hardening phenomenon is also displayed in Fig. 5(a) for a more complicated loading condition. The cyclic hardening is obvious at the first few cycles, and steadily decreases with increasing amplitude of strain cycles.

3.2.6. Erasure of memory

It is well recognized that material always has a certain memory of the history of plastic deformation it experienced. However, under some circumstances the plastic response may become independent of its previous deformation history. This property has been observed in real materials and referred to as the property of erasure-of-memory (Lamba and Sidebottom, 1978; Dafalias, 1984).

From Eq. (14) it can be seen that τ_y^m has a memory of the latest reversal stress point $\mathbf{s}(t_{\text{off}})$. In Fig. 7, we show a stress–strain curve with $\tau_y^0 = 200$ MPa and $\rho = 1.5$. The monotonic loading curve of the original model is the boundary of all other unloading–reloading curves of the new model, and is an invariant curve as demonstrated above. The loading–unloading–reloading curve, which interrupts by an elastic unloading–reloading piece, will eventually approach to the monotonic loading curve if there has an enough loading time as shown in Fig. 7. Obviously, this property of erasure-of-memory follows from the existence of equilibrium stress point associated with the new model. More explicitly speaking, for each big strain loading the existence of equilibrium stress point brings the material back to that stress state regardless of the previous response history.

In the calculation of the elastic unloading–reloading curve of AB in Fig. 7, we need to define a new yield stress level at point A denoted by $\tau_y^A = \|\mathbf{s}_A\|/\sqrt{2}$. When an elastic loading starts from point B, the switch-on time is calculated by Eq. (7) but with τ_y^0 replaced by τ_y^A. Doing so the stress path will trace along BA and yield at point A again to continue the plastic loading curve. In this elastic unloading–reloading case the smoothing factor is taken to be $\rho = 1$; otherwise, we may obtain an incorrect "open hysteresis" loop.

3.2.7. Mean-stress relaxation

Under unsymmetric strain cycles it is experimentally observed that the mean stress of materials is gradually relaxed to zero. In Fig. 8, where $\tau_y^0 = 400$ MPa and $\rho = 2$ were used, we subject the new model to the

[4] Dafalias (1984) has experimentally observed that the reverse yielding occurs before even the tensile stress changes to compressive for grade 60 steel. To model such a strong Bauschinger effect of material we may need to consider kinematic hardening in the new model (see Section 5).

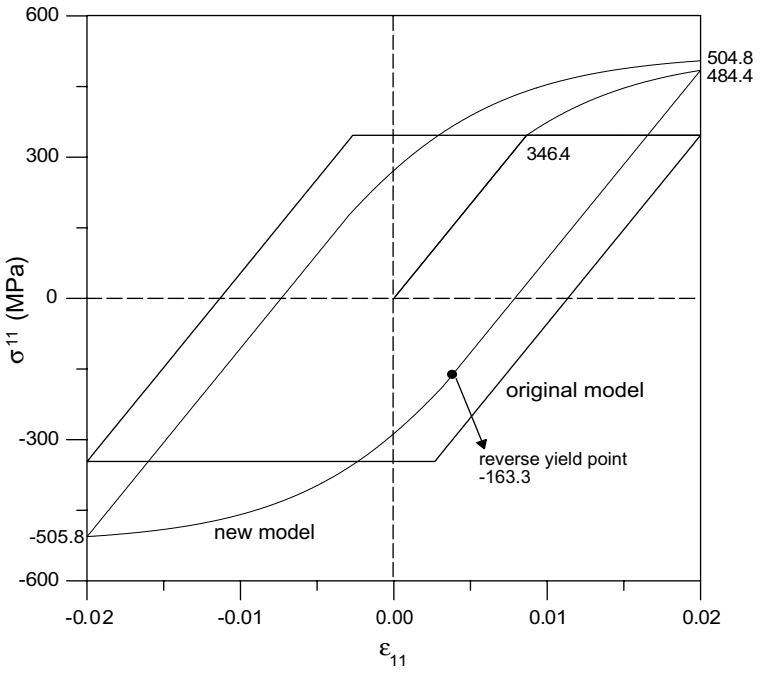

Fig. 6. The uniaxial behavior of the original model and the new model within one strain cycle. The Bauschinger effect and cyclic hardening only revealed by the new model.

unsymmetric strain cycles with amplitude 0.01 and mean 0.01. The time history of axial stress is shown in Fig. 8(a), and the stress–strain curve is shown in Fig. 8(b), from which we can see that the new model is able to properly reflect the relaxation of mean stress. On the other hand, let us compare Fig. 3(e) and (k) again, both subject to the same unsymmetric strain cycles as shown in Fig. 3(d). As can be seen from Fig. 3(e), the stress–strain curve of the original model does not reveal any mean-stress relaxation; conversely, the stress–strain curve of the new model exhibits a mean-stress relaxation as shown in Fig. 3(k).

3.2.8. Strain ratcheting

Substituting Eq. (12) for $\dot{\lambda}$ into Eq. (1) we get

$$\dot{\mathbf{s}} = 2G\left[\mathbf{I} - \frac{\mathbf{s}\otimes\mathbf{s}}{2(\tau_y^0)^2}\right]\dot{\mathbf{e}}, \tag{22}$$

where $\mathbf{I}$ is a fourth-order identity tensor and $\otimes$ denotes the tensor product. Taking the inverse of the above equation, we obtain

$$\dot{\mathbf{e}} = \frac{1}{2G}\left[\mathbf{I} + \frac{\mathbf{s}\otimes\mathbf{s}}{2(\tau_y^0)^2 - \|\mathbf{s}\|^2}\right]\dot{\mathbf{s}}. \tag{23}$$

However, for the original model the above inverse is not permitted, because the normal-yield condition of $\|\mathbf{s}\|^2 = 2(\tau_y^0)^2$ will make the fourth-order elastoplastic modulus tensor singular (Liu, 2000). Therefore, the original model does not allow stress control, and a material model of this sort is instability in the sense of Drucker (1959). Conversely, the new model allows stress control in the range of $\|\mathbf{s}\|^2 < 2(\tau_y^0)^2$, which can be applied to the modeling of strain ratcheting behavior. The elastoplastic modulus tensor for the new model is positive definite, and hence is stable in the sense of Drucker (1959).

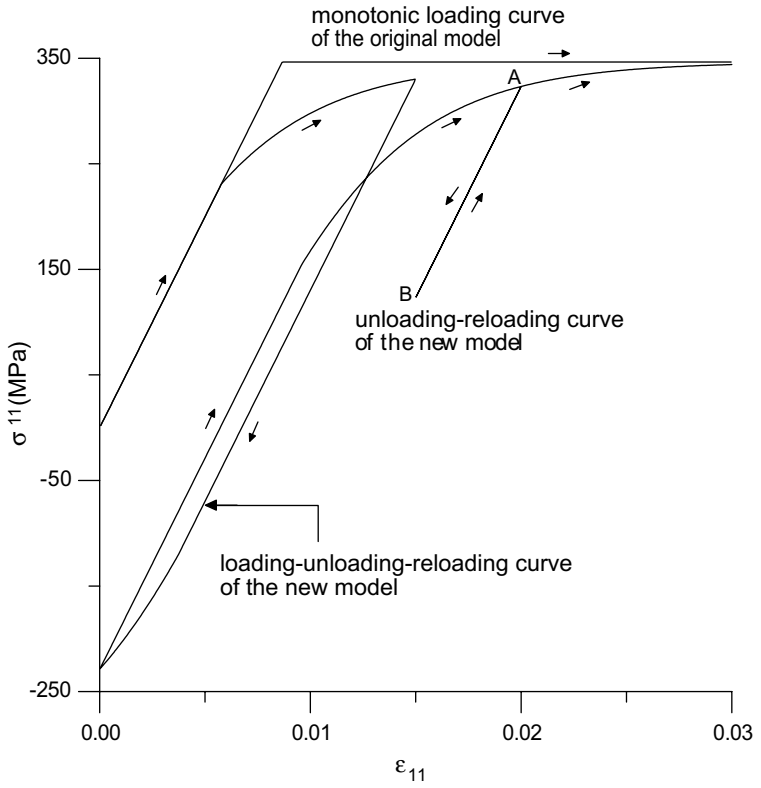

Fig. 7. The monotonic loading curve of the original model is a limiting curve of any loading–unloading–reloading curves of the new model.

It is experimentally observed that unsymmetric stress cycles will cause a cyclic creep of strain in the direction of mean stress, also called strain ratcheting behavior. In Fig. 9, we show the uniaxial cyclic stress–strain curves for different initial pre-stresses of σ_{11} but with $\tau_y^0 = 400$ MPa and $\rho = 2$ being kept constant for all cases. It shows that the new model is able to reveal the strain ratcheting behavior; furthermore, it is observed that the symmetric stress cycles with a zero mean stress gives no strain ratcheting as shown in Fig. 9(a) and (b), and a larger mean-stress leads to a larger strain ratcheting as shown in Fig. 9(c)–(h).

The above results are calculated by integrating Eq. (23) of the plastic phase together with the elastic phase equation $\dot{\mathbf{e}} = \dot{\mathbf{s}}/(2G)$ under the stress control of $\mathbf{s}(t)$. By considering a rectilinear stress path specified by $\dot{\mathbf{s}} = \mathbf{C}$ with $\mathbf{C}$ a constant deviatoric tensor, the integration of Eq. (23) leads to

$$\mathbf{e}(t) = \mathbf{e}(t_{\text{on}}) + \left[\frac{B\mathbf{C}}{8GA} - \frac{\mathbf{s}(t_{\text{on}})}{4G}\right] \ln \frac{A(t-t_{\text{on}})^2 + B(t-t_{\text{on}}) + C}{C} - \frac{\mathbf{C}\sqrt{B^2-4AC}}{8GA} \times \ln \frac{[2A(t-t_{\text{on}}) + B - \sqrt{B^2-4AC}][B+\sqrt{B^2-4AC}]}{[2A(t-t_{\text{on}}) + B - \sqrt{B^2-4AC}][B-\sqrt{B^2-4AC}]}, \tag{24}$$

where

$$A := \|\mathbf{C}\|^2, \quad B := 2\mathbf{s}(t_{\text{on}}) \cdot \mathbf{C}, \quad C := \|\mathbf{s}(t_{\text{on}})\|^2 - 2(\tau_y^0)^2. \tag{25}$$

Similarly, the same strategy of shortening the switch-on time t_{on} by a factor ρ is applied for this control case.

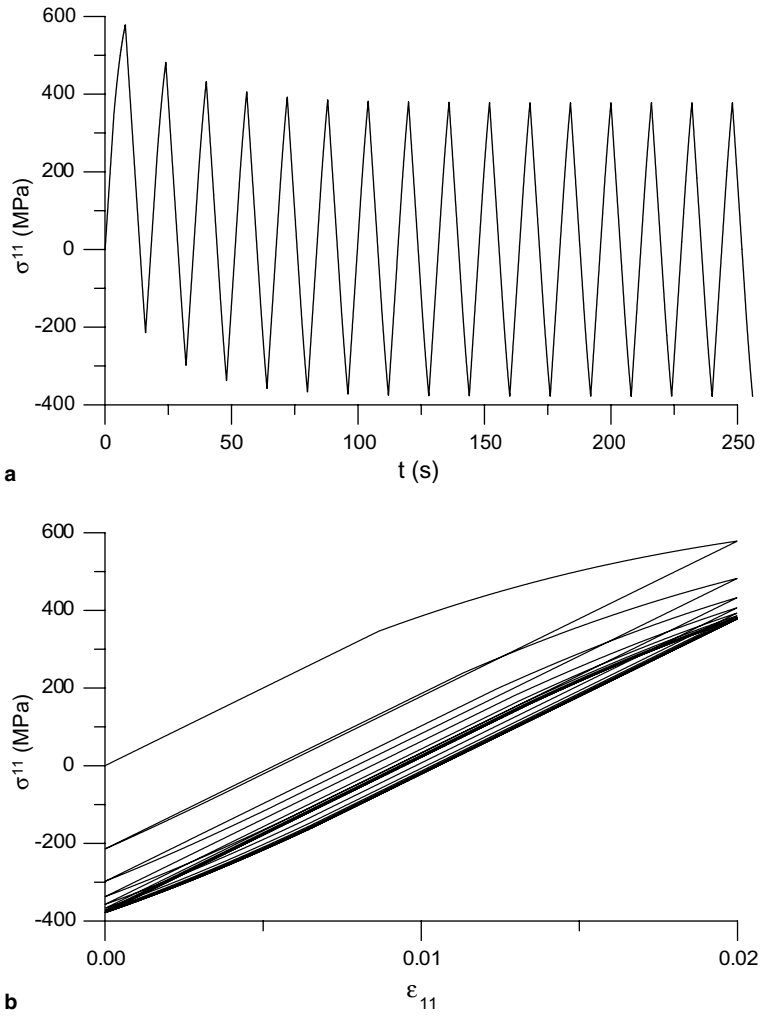

Fig. 8. Mean-stress relaxation of the new model under the unsymmetric strain cycles: (a) time history of axial stress and (b) stress–strain curve.

The experimental uniaxial/multiaxial ratcheting tests of metals were carried out by many researchers (for example, Jiang and Sehitoglu, 1994a,b; Delobelle et al., 1995; McDowell, 1995; Mizuno et al., 2000; Kang et al., 2002a,b; Kang and Gao, 2002; and references therein). A major observation of the ratcheting behavior for most metals is the ratcheting rate decreasing cyclically and then stopping.

The new model was modified merely from a simple perfectly elastoplastic model, which even was able to simulate the strain ratcheting and mean stress relaxation phenomena as discussed above, it over predicts these two behaviors. In fact Fig. 7 shows the weakness of this model, namely that upon unloading, partial reverse loading and reloading in the initial direction, a strong undershooting of the initial plastic loading curve takes place. This usually leads to an excessively large ratcheting effect as shown in Fig. 9, or a large mean-stress relaxation as shown in Fig. 8. How to remedy these drawbacks becomes an important issue for the new model. For this we turn our attention to the smoothing factor which plays an important role in the modification, and about which we should note that a smaller ρ is, a more close to the original perfectly

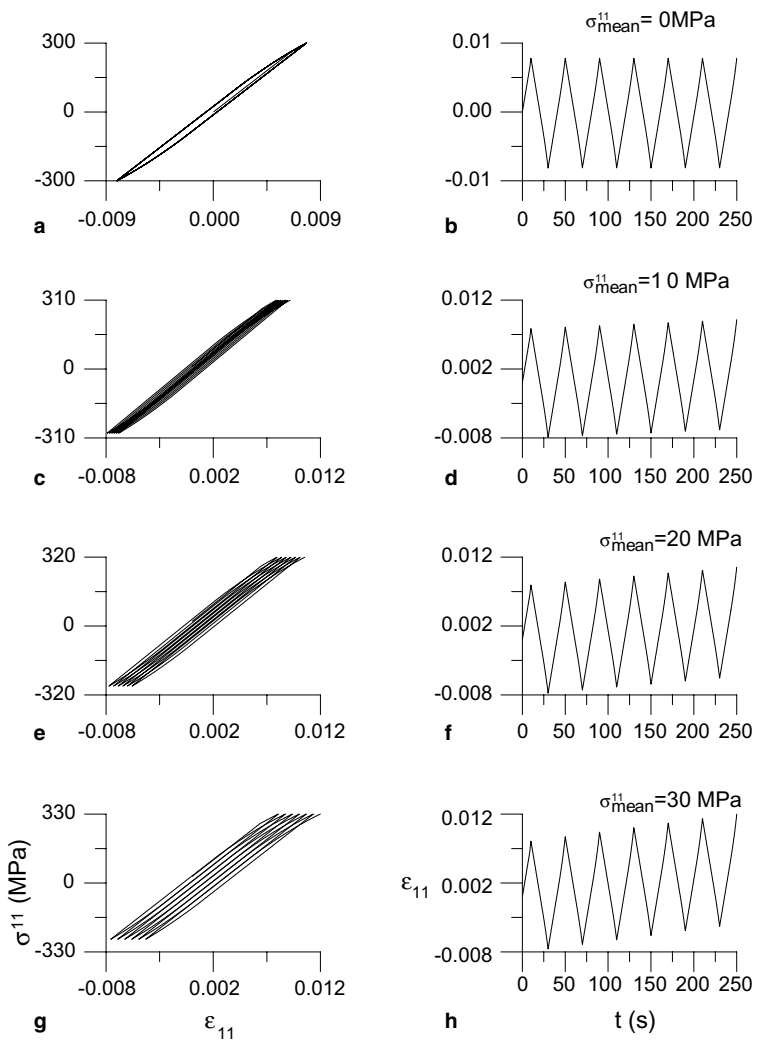

Fig. 9. Under unsymmetric stress cycles the strain ratcheting behavior for the new model is shown for different mean stresses. A larger mean stress renders a larger strain ratcheting.

elastoplastic model will be, deviating from the aim of the description of cyclic plasticity and ratcheting effect. On the other hand, a larger ρ is, a more profound ratcheting effect reveals. In order to suppress the ratcheting and relaxation effects, and get a trade-off between these two tendencies we may decrease the value of ρ from a larger value ρ_2 to a smaller value ρ_1 by letting (Liu and Chang, 2005)

$$\rho(\lambda) = \rho_1 + (\rho_2 - \rho_1)\exp(-k\lambda), \quad 1 \leqslant \rho_1 \leqslant \rho_2 \leqslant 2. \tag{26}$$

Instead of the constant ρ used in the above simulations as shown in Figs. 8 and 9, we supposed that the smoothing factor ρ is a scalar function of λ, which is calculated by

$$\lambda(t) = \lambda(t_{\text{on}}) + \frac{\tau_y^0}{2G}\ln\frac{2(\tau_y^0)^2 - \|\mathbf{s}(t_{\text{on}})\|^2}{2(\tau_y^0)^2 - \|\mathbf{s}(t)\|^2} \tag{27}$$

under a stress control. In Fig. 10(a), the uniaxial ratchetings under a mean stress of 50 MPa and a stress amplitude of 300 MPa are compared by fixing $\rho = 2$ (dashed line) and by employing a scalar function for ρ with $\rho_1 = 1$, $\rho_2 = 2$ and $k = 50$ in Eq. (26). The latter result is shown by a solid line, which can be seen that the ratcheting rate decreases cyclically and the ratcheting stops almost at the 10th cycle. The total ratcheting strain is about one-half of the former one that used $\rho = 2$. To simulate the biaxial ratcheting, the stress loading condition is a constant shear stress $\sigma_{12} = 50$ MPa combined with an unsymmetrical axial stress σ_{11} cycling with a mean stress of 50 MPa and stress amplitude of 300 MPa. The calculations show that the biaxial ratcheting takes place not only in the torsional direction but also in the axial direction due to the constant shear stress and a non-zero mean axial stress. However, the case with a fixed $\rho = 2$ (dashed line) leads to constant ratcheting rates in that two directions and usually over predicts the ratcheting strains. By using the same strategy as above we obtain a more reasonable biaxial ratcheting simulated result as shown by the solid line in Fig. 10(b).

By adjusting the three constants of ρ_1, ρ_2 and k in Eq. (26) we may observe different ratcheting behaviors. Although the replacement of a constant ρ by a scalar function ρ may increase a little of computational

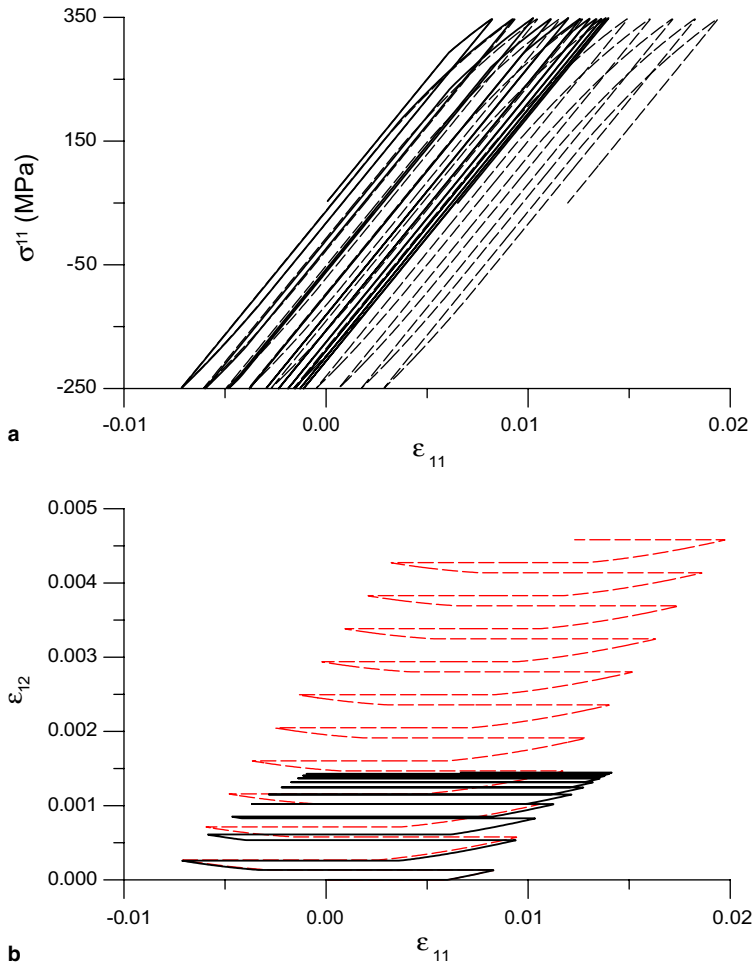

Fig. 10. By employing a scalar function for the smoothing factor in the new model renders a more effective simulation of (a) uniaxial and (b) biaxial ratcheting behaviors under the unsymmetric stress loadings.

burden but its effect is increased remarkably. It deserves to note that our model includes no kinematic hardening variables in the formulation. The description of ratcheting in terms of constitutive equations is usually related to the kinematic hardening mechanism. Several experimental and numerical studies on metals have shown the inability of the classical kinematic hardening rules to describe the main ratcheting phenomenon. However, a correct simulation of ratcheting phenomena is still one of the most difficult problems, and there are more accurate and realistic but complex constitutive models that allow to simulate the ratcheting more appropriately (for example, Chaboche, 1991, 1994; Voyiadjis and Sivakumar, 1991, 1994; Hassan and Kyriakides, 1992; Ohno and Wang, 1993, 1994; Jiang and Sehitoglu, 1994a,b; Delobelle et al., 1995; Corona et al., 1996; Xia and Ellyin, 1997; Chaboche and Jung, 1998; Taheri and Lorentz, 1999; Abdel-Karim and Ohno, 2000; Ohno and Abdel-Karim, 2000; Portier et al., 2000; Bari and Hassan, 2001, 2002). The above lists just reflect an active studying issue of the ratcheting behavior, and the improvements are still in progress.

3.2.9. Continuous plastic modulus

Recalling the decomposition of $\dot{\mathbf{e}} = \dot{\mathbf{e}}^{\mathrm{e}} + \dot{\mathbf{e}}^{\mathrm{p}}$ and the elastic relation of $\dot{\mathbf{e}}^{\mathrm{e}} = \dot{\mathbf{s}}/(2G)$, and noting the positive definiteness of $\mathbf{s} \otimes \mathbf{s}$ in the plastic phase, from Eq. (23) it follows that

$$\dot{\mathbf{s}} = 2G[2(\tau_y^0)^2 - \|\mathbf{s}\|^2](\mathbf{s} \otimes \mathbf{s})^{-1}\dot{\mathbf{e}}^{\mathrm{p}}. \tag{28}$$

The fourth-order tensor $2G[2(\tau_y^0)^2 - \|\mathbf{s}\|^2](\mathbf{s} \otimes \mathbf{s})^{-1}$ is the plastic modulus tensor of the new model.

In terms of the unit tensor $\mathbf{n} := \mathbf{s}/\|\mathbf{s}\|$ the plastic strain is determined by the flow rule:

$$\dot{\mathbf{e}}^{\mathrm{p}} = \frac{1}{K_p}(\mathbf{n} \cdot \dot{\mathbf{s}})\mathbf{n} \tag{29}$$

with

$$K_p = \frac{2G[2(\tau_y^0)^2 - \|\mathbf{s}\|^2]}{\|\mathbf{s}\|^2} \tag{30}$$

a scalar plastic modulus, which varies continuously in the following range:

$$0 < K_p \leqslant \frac{2G[2(\tau_y^0)^2 - 2(\tau_y^m)^2]}{2(\tau_y^m)^2}. \tag{31}$$

In terms of the ratio of $R := \|\mathbf{s}\|/(\sqrt{2}\tau_y^0)$, we can rewrite Eq. (30) to

$$K_p = \frac{2G(1-R^2)}{R^2}. \tag{32}$$

This equation indicates that the scalar plastic modulus approaches zero when stress tends to limiting surface, and that the scalar plastic modulus approaches infinity when yielding happens for a zero stress.

3.3. Comments on the new model and others

The use of τ_y^m in the new model reflects a discrete memory of the most recent unloading–reloading event. However, τ_y^m has to be updated according to Eq. (14) when each time a change in the loading direction occurs.

Unlike the multi-surface model of Mróz (1967), whose predicted stress–strain curve is piecewise linear because of the field of constant plastic moduli and to produce a smooth non-linear curve which requires a large number of nesting subyield surfaces, our model gives a smooth stress–strain curve due to the continuous variation of the plastic modulus tensor. On the other hand, the Mróz model gives no ratcheting at all and cannot describe the mean stress relaxation; refer the comments by Ristinmaa (1995), McDowell (1995), Jiang and Sehitoglu (1996) and Bari and Hassan (2000).

What it appears to be peculiar of the new model is that when an unloading occurs, the stress point at unloading is kept in memory as a new reference point from which the new elastic range is constructed through a smoothing factor specified. We should stress that this elastic range is not centered at the unloading point, but it is biased towards the new direction of loading. A somewhat similar concept has been used by Mróz et al. (1981) and Klisiński and Mróz (1988) to an infinite number of nesting surfaces model, where the ratio of the size of a current loading surface, eccentrically placed with respect to the latest unloading point, to the size of the normal-yield surface, plays the role of an interpolation factor, and then the plastic modulus is a function of this ratio and the plastic hardening modulus at the conjugate point on the normal-yield surface. This model requires to memorize the normal-yield surface, active loading surface as well as many stress reversal surfaces. Therefore, the numerical computation is not always simple. Furthermore, as noted by Hashiguchi (1993) the infinite surface model may have singular plastic moduli field, leading to excessively large hysteresis loop and an incapability of describing the strain ratcheting.

The mathematical features of the two-surface model proposed by Dafalias and Popov (1975) are two-fold. A single subyield surface enclosing a purely elastic domain is assumed within the normal-yield surface, which translates in a loading process, keeping a similarity to each other and a ratio of similarity to be constant. The plastic modulus is then given by a monotonically increasing function of the distance from a current loading stress point on the subyield surface to a conjugate point on the normal-yield surface. At these two points the two surfaces have the same outward normal. The two-surface model can satisfy all the five requirements listed in Section 1. One of the disadvantages of this model is that it needs a significant memory capability for updating the procedures in computations. Chaboche (1986) has pointed out its inconsistency in the uniaxial loading–unloading–reloading situations where plastic flow is very small during reloading. This leads to an overshooting of the subsequent tensile curve. In addition, this model also predicts excessively small or open hysteresis loop so that leads to an extremely strong ratcheting effect.

The subloading surface model proposed and refined by Hashiguchi (1989) assumed that the subloading surface expands or contracts passing always through a current stress point no matter in loading or in unloading states and retaining a geometrical similarity to the normal-yield surface, and is the description of a plastic modulus by the ratio of the size of the subloading surface to that of the normal-yield surface. This model does not exist elastic domain and the plastic modulus changes continuously. Elasticity only happens for the unloading case. In addition to the memorization of normal-yield surface and subloading surface this model requires to formulate the evolution equations for the similarity center and for the other two centers of normal-yield surface and subloading surface. Even this model does not require the judgement whether a stress lies on the yield surface or not, it requires a lot of computations to trace the evolutions of these surfaces.

From the above discussions it is clear that the new model is different from the two-surface model, the infinite-surface model and the subloading surface model. The basic idea in the new model is allowing plasticity to happen inside the normal-yield surface, and the method is to shorten the switch-on time by a factor $\rho > 1$. Its formulations are simpler than the above mentioned unconventional models, and its numerical implementation is more easy without memorizing the evolution of any surface. The existence of a limiting surface is a natural result without specifying any evolution rule on it.

4. A natural strain-hardening mechanism of the new model

4.1. The underlying space of the new model

Sometimes we may need to calculate the responses under a more general strain path for the sake of model simulation or experimental identification. For this purpose the following linear representation of the flow model is very useful (Hong and Liu, 1997, 2000):

$$\dot{\mathbf{X}} = \mathbf{A}\mathbf{X}, \tag{33}$$

where

$$\mathbf{X} = \begin{bmatrix} \mathbf{X}^s \\ X^0 \end{bmatrix} := \frac{X^0}{\tau_y^0} \begin{bmatrix} a_1 s^{11} + a_2 s^{22} \\ a_3 s^{11} + a_4 s^{22} \\ s^{23} \\ s^{13} \\ s^{12} \\ \tau_y^0 \end{bmatrix} \tag{34}$$

is the augmented stress,

$$X^0 := \exp\left(\frac{\lambda}{\gamma_y}\right) \tag{35}$$

is the integrating factor of Eq. (1), and

$$a_1 := \sin\left(\varphi + \frac{\pi}{3}\right), \quad a_2 := \sin\varphi, \quad a_3 := \cos\left(\varphi + \frac{\pi}{3}\right), \quad a_4 := \cos\varphi \tag{36}$$

with φ being any real number. The system matrix $\mathbf{A}$ is subjected to the following switch criteria for plastic and elastic phases:

$$\mathbf{A} = \begin{bmatrix} \mathbf{0}_{5\times5} & \mathbf{A}_0^s \\ \mathbf{A}_s^0 & 0 \end{bmatrix} \quad \text{if } 0 > \mathbf{X}^{\mathrm{T}}\mathbf{g}\mathbf{X} \geqslant \left[\left(\frac{\tau_y^m}{\tau_y^0}\right)^2 - 1\right] \text{ and } \frac{\mathrm{d}}{\mathrm{d}t}\left[(\mathbf{X}^s)^{\mathrm{T}}\mathbf{X}^s\right] > 0, \tag{37}$$

$$\mathbf{A} = \begin{bmatrix} \mathbf{0}_{5\times5} & \mathbf{A}_0^s \\ \mathbf{0}_{1\times5} & 0 \end{bmatrix} \quad \text{if } \mathbf{X}^{\mathrm{T}}\mathbf{g}\mathbf{X} < \left[\left(\frac{\tau_y^m}{\tau_y^0}\right)^2 - 1\right] \text{ or } \frac{\mathrm{d}}{\mathrm{d}t}\left[(\mathbf{X}^s)^{\mathrm{T}}\mathbf{X}^s\right] \leqslant 0, \tag{38}$$

in which

$$\mathbf{A}_0^s := \frac{2}{\gamma_y} \begin{bmatrix} a_1\dot{e}_{11} + a_2\dot{e}_{22} \\ a_3\dot{e}_{11} + a_4\dot{e}_{22} \\ \dot{e}_{23} \\ \dot{e}_{13} \\ \dot{e}_{12} \end{bmatrix}, \tag{39}$$

$$\mathbf{A}_s^0 = (\mathbf{A}_0^s)^{\mathrm{T}}, \tag{40}$$

and

$$\mathbf{g} = \begin{bmatrix} \mathbf{I}_5 & \mathbf{0}_{5\times1} \\ \mathbf{0}_{1\times5} & -1 \end{bmatrix} \tag{41}$$

a Minkowski metric tensor.

The space $\mathbf{X}$ endowed with the metric tensor $\mathbf{g}$ is usually called the Minkowski spacetime (Liu, 2001). For the original model in the plastic phase its augmented stress vector is a null vector on the cone $\{\mathbf{X}|\mathbf{X}^{\mathrm{T}}\mathbf{g}\mathbf{X} = 0\}$. However, for the new model in the plastic phase the augmented stress vector is a time-like vector inside the cone, i.e., $\{\mathbf{X}|\mathbf{X}^{\mathrm{T}}\mathbf{g}\mathbf{X} < 0\}$, as can be seen from Eq. (37). In Fig. 11, we show the underlying spaces for the original model and for the new model in the three-dimensional space of (X^1, X^2, X^0). The underlying space for the original model is a truncated cone, and the underlying space for the new model is truncated hyperboloids. In each plastic loading case the augmented stress orbit may lie on different hyperboloids.

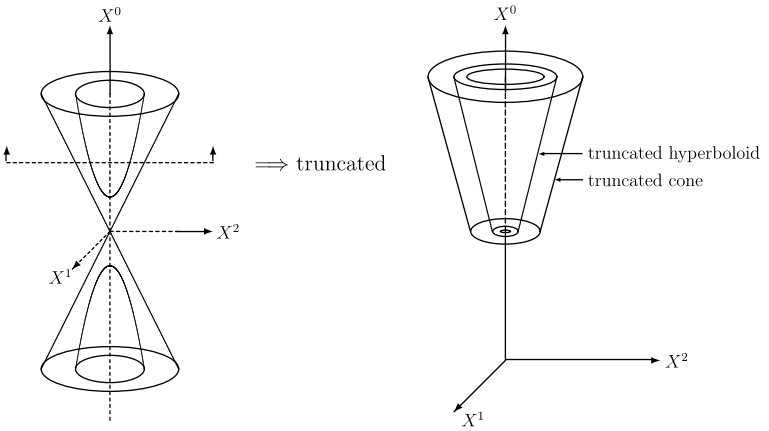

Fig. 11. The two geometric sets of $\mathbf{X}^{\mathrm{T}}\mathbf{g}\mathbf{X} = -r$ and $X^0 \geqslant 1$. Depending on the value of r the set is one of truncated hyperboloid of two sheets or truncated cone. The truncated plane is taken at $X^0 = 1$.

Now we prove that

$$\mathbf{X}^{\mathrm{T}}\mathbf{g}\mathbf{X} = \left[\left(\frac{\tau_y^m}{\tau_y^0}\right)^2 - 1\right] < 0 \tag{42}$$

is an invariant set of Eq. (33) for each plastic phase (Hong and Liu, 1999). Taking the time derivative of $\mathbf{X}^{\mathrm{T}}\mathbf{g}\mathbf{X}$ and substituting Eq. (33) for $\dot{\mathbf{X}}$ and then noting that

$$\mathbf{A}^{\mathrm{T}}\mathbf{g} + \mathbf{g}\mathbf{A} = \mathbf{0} \tag{43}$$

by Eq. (37), we obtain

$$\frac{\mathrm{d}}{\mathrm{d}t}[\mathbf{X}^{\mathrm{T}}\mathbf{g}\mathbf{X}] = 0, \tag{44}$$

which means that $\mathbf{X}^{\mathrm{T}}\mathbf{g}\mathbf{X}$ is a constant during the plastic phase, and hence Eq. (42) holds for each plastic phase until an unloading occurs. On the other hand, from Eq. (43) we know that $\mathbf{A}$ is a Lie algebra of the proper orthochronous Lorentz group, which together with Eqs. (42), (34), (41) and (35) lead to the following important result:

$$\|\mathbf{s}\|^2 = 2(\tau_y^0)^2 + \left[2(\tau_y^m)^2 - 2(\tau_y^0)^2\right] \exp\left(\frac{-2\lambda}{\gamma_y}\right). \tag{45}$$

Mathematically speaking, the new model has a natural strain-hardening law, and Eq. (45) is the unique strain-hardening law that admits a Minkowski spacetime structure on the augmented stress X, on which the proper orthochronous Lorentz group left acts.

The above result is rather significant, which says that for the new model in each plastic phase it can harden from an initial shear yield strength of τ_y^m to a saturated shear strength of τ_y^0 with a hardening rate of $2/\gamma_y$. Very interestingly, the new model possesses a natural hardening mechanism specified by Eq. (45). This is however impossible for the original model, of which the hardening term as given by $[2(\tau_y^m)^2 - 2(\tau_y^0)^2]$ $\exp(-2\lambda/\gamma_y)$ disappears. Especially, the new model still exhibits an internal symmetry group of $SO_{\mathrm{o}}(5,1)$ as the original model has (Hong and Liu, 1999, 2000).

4.2. The group-preserving scheme

To obtain $\mathbf{s}$ the calculation of $\mathbf{X}$ is sufficient in view of Eq. (34), and we do not need to carry the more complex numerical solutions of Eqs. (1), (12) and (13). Because $\mathbf{A}$ as shown in Eq. (37) is time-dependent, the closed-form solution of $\mathbf{X}$ is usually not available. However, the group property as the new model has may help us to devise a very efficient and accurate numerical scheme as follows.

Now let us consider a general strain path $\mathbf{e}(t)$, and we want to find the responses of the new model. To devise a numerical scheme for the time-marching integration, let us denote the time increment by Δt and develop a mapping to update $\mathbf{s}(t)$ to the next time step $\mathbf{s}(t+\Delta t)$. We may approximate a general strain path by many piecewise rectilinear strain paths as follows:

$$\mathbf{e}(t+\Delta t) = \mathbf{e}(t) + \dot{\mathbf{e}}(t)\Delta t.$$

For each $\dot{\mathbf{e}}(t)$ we map it to the corresponding $\mathbf{A}_0^s(t)$ via Eq. (39), and then calculate $\exp[\mathbf{A}(t)\Delta t]$ in order to calculate $\mathbf{X}(t+\Delta t)$ from $\mathbf{X}(t)$. It can be determined exactly (see, e.g., Hong and Liu, 2000), such that a numerical scheme for the plastic phase can be derived as follows:

$$\mathbf{X}(t+\Delta t) = \mathbf{G}(t+\Delta t)\mathbf{G}^{-1}(t)\mathbf{X}(t), \tag{46}$$

where

$$\mathbf{G}(t+\Delta t)\mathbf{G}^{-1}(t) = \begin{bmatrix} \mathbf{I}_5 + \dfrac{a-1}{\|\mathbf{A}_0^s(t)\|^2}\mathbf{A}_0^s(t)\mathbf{A}_s^0(t) & \dfrac{b\mathbf{A}_0^s(t)}{\|\mathbf{A}_0^s(t)\|} \\ \dfrac{b\mathbf{A}_s^0(t)}{\|\mathbf{A}_0^s(t)\|} & a \end{bmatrix}, \tag{47}$$

in which

$$a := \cosh(\Delta t\|\mathbf{A}_0^s(t)\|), \quad b := \sinh(\Delta t\|\mathbf{A}_0^s(t)\|). \tag{48}$$

Upon knowing $\mathbf{X}(t+\Delta t)$ we can use

$$\begin{bmatrix} s^{11} \\ s^{22} \\ s^{23} \\ s^{13} \\ s^{12} \end{bmatrix} = \begin{bmatrix} a_4 & -a_2 & \mathbf{0}_{2\times 3} \\ -a_3 & a_1 & \\ \mathbf{0}_{3\times 2} & & \frac{\sqrt{3}}{2}\mathbf{I}_3 \end{bmatrix} \frac{2\tau_y^0}{\sqrt{3}X^0}\mathbf{X}^s \tag{49}$$

to calculate the deviatoric stress tensor of $\mathbf{s}(t+\Delta t)$.

In order to smooth the response curves we need to calculate the switching-on time for the general strain path. Substituting the elastic equation

$$\mathbf{s}(t) = \mathbf{s}(t_{\text{off}}) + 2G[\mathbf{e}(t) - \mathbf{e}(t_{\text{off}})] \tag{50}$$

into the yield condition $\|\mathbf{s}(t)\|^2 = 2(\tau_y^0)^2$ generates usually a non-linear equation for t as follows:

$$\|\mathbf{s}(t_{\text{off}})\|^2 + 4G\mathbf{s}(t_{\text{off}})\cdot[\mathbf{e}(t) - \mathbf{e}(t_{\text{off}})] + 4G^2\|\mathbf{e}(t) - \mathbf{e}(t_{\text{off}})\|^2 - 2(\tau_y^0)^2 = 0. \tag{51}$$

Solve this equation numerically and denote the solution by t_{on}^0. Then we replace it by a new switching-on time

$$t_{\text{on}} = t_{\text{off}} + \frac{t_{\text{on}}^0 - t_{\text{off}}}{\rho}. \tag{52}$$

After this time the new model is in the plastic phase, and the numerical scheme (46) is used to calculate the response until an unloading occurs. Even for calculating the responses under a general strain path the numerical implementation of the new model is still rather straightforward and highly efficient. Below we give an numerical example to display the out-of-phase hardening effect of the new model under a non-proportional two-dimensional strain path.

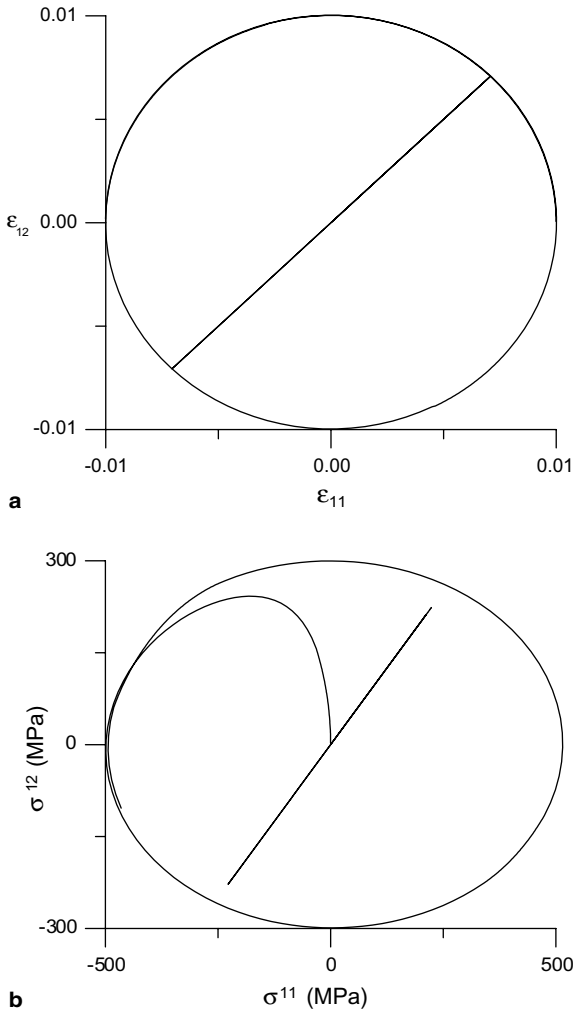

Fig. 12. Displaying an out-of-phase hardening of the new model: (a) proportional and non-proportional circular strain paths with the same amplitude and (b) corresponding stress paths.

4.2.1. Out-of-phase hardening

By using the above scheme we can calculate the responses of the new model under a proportional strain path and a 90° out-of-phase strain path with the same amplitude as shown in Fig. 12(a), where $\tau_y^0 = 300$ MPa and $\rho = 2$ were used. During the multiaxial cyclic loading, materials generally show significantly a higher stress level than in the proportional deformation loading. The out-of-phase hardening as shown in Fig. 12(b) is enhanced by the out-of-phase strain path.

5. Comparisons with experimental data

As indicated in Fig. 6 the new model can describe a little of the Bauschinger effect; however, in order to enhance the simulation capability it needs the model being able to describe the kinematic hardening more closely. In many metals subjected to cyclic loadings, it is experimentally observed that the center of yield surface experiences a large motion in the direction of plastic flow. This hardening behavior is known as the Bauschinger effect.

A simple phenomenological description that captures the Bauschinger effect is constructed by introducing an additional internal tensorial variable of $\mathbf{s}_b$ called the back stress, which defines the current center of the yield surface and is supposed to be governed by Prager (1956) kinematic hardening rule:

$$\dot{\mathbf{s}}_b = 2k'\dot{\mathbf{e}}^p, \tag{53}$$

where the material constant k' is the kinematic modulus in shear deformation. The relative stress $\mathbf{s}_a$ is defined as the difference of stress and back stress:

$$\mathbf{s}_a = \mathbf{s} - \mathbf{s}_b. \tag{54}$$

The above two equations together with the elastic equation $\dot{\mathbf{s}} = 2G[\dot{\mathbf{e}} - \dot{\mathbf{e}}^p]$ lead to

$$\dot{\mathbf{s}}_b = \frac{2Gk'}{G+k'}\dot{\mathbf{e}} - \frac{k'}{G+k'}\dot{\mathbf{s}}_a, \tag{55}$$

integrating which we obtain

$$\mathbf{s}_b(t) = \mathbf{s}_b(t_{on}) + \frac{2Gk'}{G+k'}[\mathbf{e}(t) - \mathbf{e}(t_{on})] + \frac{k'}{G+k'}[\mathbf{s}_a(t_{on}) - \mathbf{s}_a(t)]. \tag{56}$$

This equation is suitably to simulate the material behavior under a strain-controlled test. $\mathbf{s}_a$ is now replaced the role of $\mathbf{s}$ in Sections 2–4 and is calculated by Eq. (9), whereas t_{on} is calculated by Eq. (15). In that two equations $\mathbf{s}$ is replaced by $\mathbf{s}_a$. When the Prager model is under the stress control we derive the strain equation in Appendix B.

After that we can use the new model together with the Prager kinematic hardening rule to simulate the experimental results reported in the literature. Shiao (2000) has conducted a series of cyclic strain loading experiments of SAE 4340 steel including two tests of constant strain amplitude of 1.5% with the means of zero and 1.5% and a test with increasing amplitude and mean, the amplitudes of which start from 0.6% to 6% by adding 0.6% per cycle and with −0.6% fixed in the compression direction. The results of response predictions using the above modified new model with the Prager kinematic hardening are shown, respectively, in Fig. 13(a)–(c). In the simulations the model parameters used were $G = 75{,}000$ MPa, $\tau_y^0 = 460$ MPa, $k' = 2000$ MPa and $\rho = 2$. It is immediately recognized that the cyclic response curves described by the new model are in good agreement with the experimental results; however, in order to simulate the experimental cyclic hardening/softening results more closely we need to consider the isotropic hardening/softening into the new model as that discussed by Liu (2003).

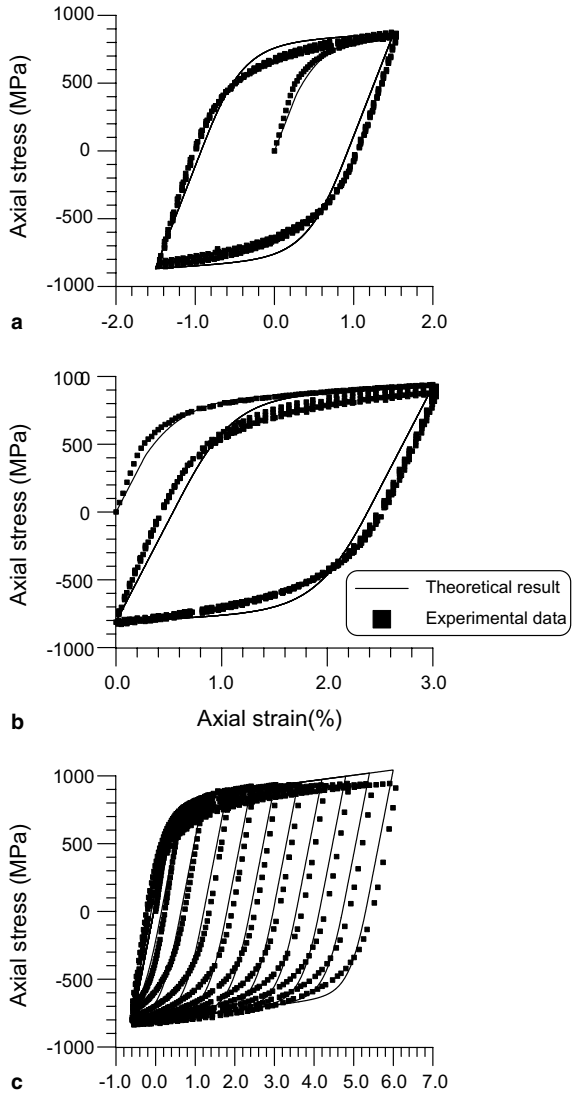

Fig. 13. The simulation of SAE 4340 steel under different axial cyclic strains.

As mentioned in Section 2, Dafalias (1984) has observed a strong Bauschinger effect for grade 60 steel. Under a random cyclic strain as shown in Fig. 14(a), which is the strain history we use in our calculation, Dafalias and Popov (1976) and Dafalias (1984) have given a very detailed description of the experimental results as shown by the solid curve in Fig. 14(b), where we are also plotted our simulation by the dashed line. In this simulation the model parameters used were $G = 13{,}000$ ksi, $\tau_y^0 = 35$ ksi, $k' = 600$ ksi and $\rho = 2$. The Arabic numbers of 1–14 appearing in Fig. 14(a) remark the turning point of the strain history. The corresponding stress–strain points are marked also in Fig. 14(b), which includes six hysteretical loops between 1–2, 3–4, 5–6, 7–8, 10–11 and 12–13. The first four loops and loop 10–11 are geometrically similar, and our simulations are closed to them; however, in the simulation of loop 12–13 our result is not so good. For this experiment, Tseng and Lee (1983) have given a rather good simulation based on the two-surface

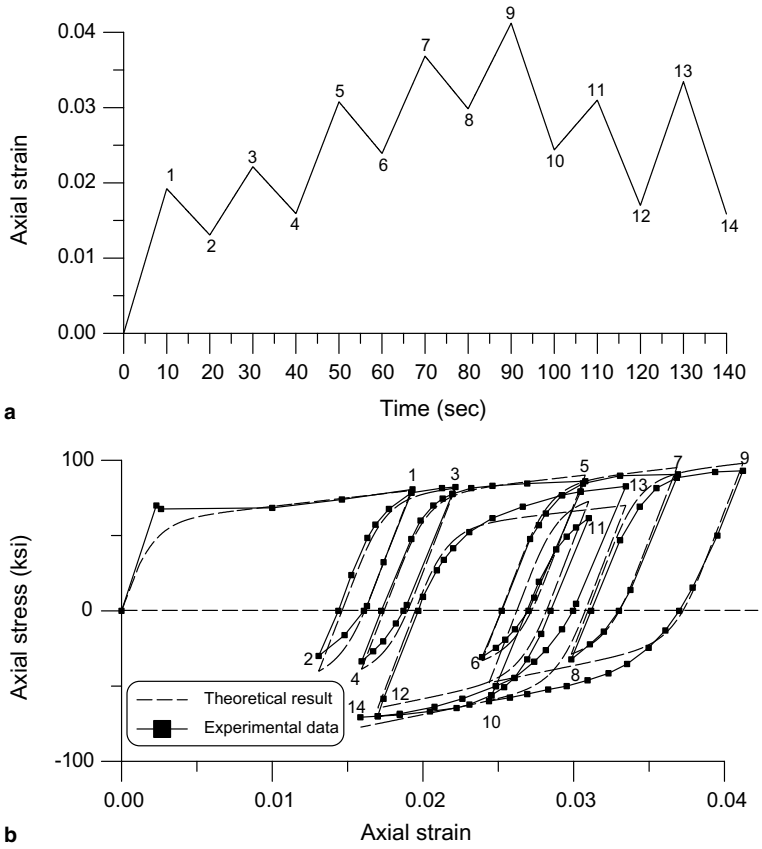

Fig. 14. The simulation of grade 60 steel under a random axial cyclic strain.

theory with stress-rate direction to find an imagined point on the memory surface. The basic idea of our model is very different from the two-surface theory. In our modified model the limiting surface is a natural result of the model, without giving an extra design of its motion. This point is different from the two-surface theory of Tseng and Lee (1983), which requires to give an evolutional law of the memory surface.

The experimental study by Kang et al. (2002a,b) indicates that SS304 stainless steel presents an obvious visco-plasticity, a significant kinematic hardening under uniaxial/multiaxial strain cycling, and an apparent fading memorization for the maximum plastic strain amplitude. The ratcheting behavior of SS304 under an unsymmetrical uniaxial stress cycling with mean axial stress of 78 MPa and stress amplitude of 248 MPa at the stress rate of 50 MPa/s was tested by Kang et al. (2002b), the stress–strain curve of which is shown in Fig. 15(a) with the dashed line. In our simulation by the new model the parameters used were $G = 72{,}180$ MPa, $\tau_y^0 = 340$ MPa, $k' = 2100$ MPa, $\rho_1 = 1.055$, $\rho_2 = 2$ and $k = 80$. The latter three parameters are used in the smoothing factor defined by Eq. (26) to gradually decrease the ratcheting rate of strain. For the axial-torsional ratcheting (Kang et al., 2002b) as shown in the right-hand side of Fig. 15(b), the loading condition is a constant shear stress of 78 MPa combined with an unsymmetrical axial stress cycling as that used in Fig. 15(a). Our simulated result is placed in the left-hand side of Fig. 15(b). The ratcheting directions of both experiment and simulation are coincident; however, the simulated axial-strain amplitude is far less than that of the experimental result. This may be due to the stress rate effect which we do not take into account in the new model.

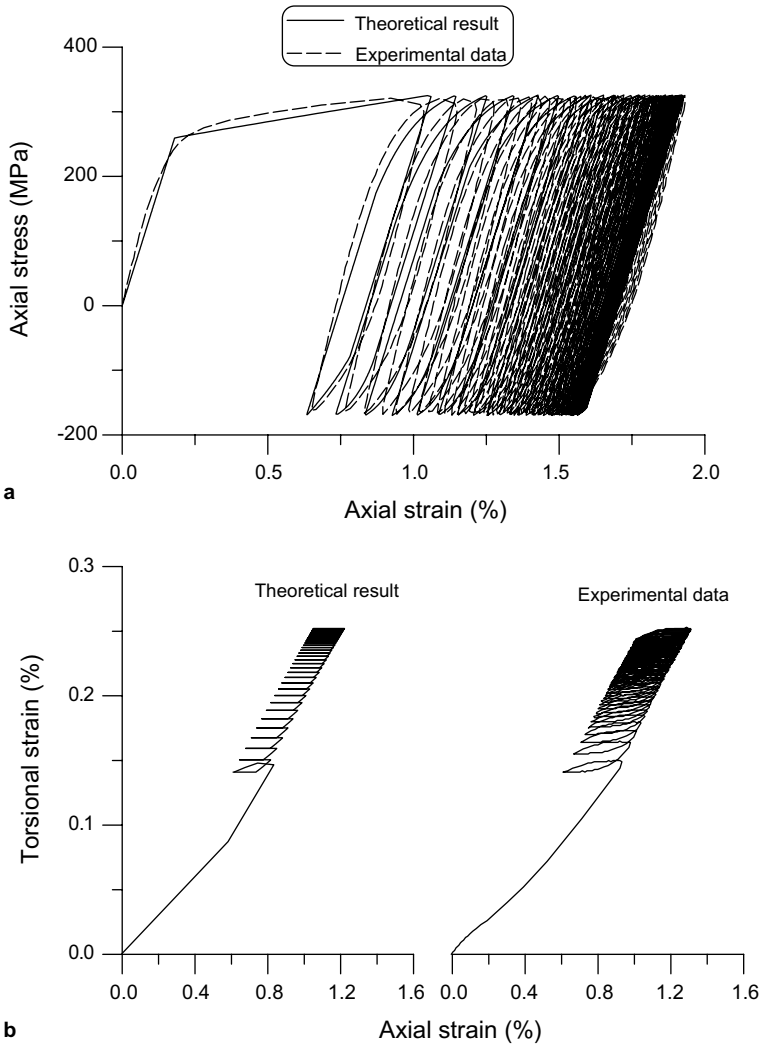

Fig. 15. The simulation of uniaxial and biaxial strain ratchetings of SS304 stainless steel.

6. Conclusions

In this paper we have proposed a simple modification of perfectly elastoplastic model by introducing a smoothing factor ρ to shorten the switch-on time. The main idea is to replace the yield surface by a new yield volume through the specification of a piecewise constant shear yield strength with $\tau_y^m < \tau_y^0$; hence, the plasticity is permitted in a non-zero-measure volume in stress space. In doing so, the mathematical equations which govern the evolution of plasticity are unchanged, but the initial stresses for plastic phase are relaxed by subjecting to $\sqrt{2}\tau_y^0 > \|\mathbf{s}\| \geqslant \sqrt{2}\tau_y^m$, not by $\|\mathbf{s}\| = \sqrt{2}\tau_y^0$ of the original model, which gives us a degree of freedom to smooth the stress–strain curves.

Moreover, we have converted the non-linear constitutive equations for the new model into a linear system for the augmented stress $\mathbf{X}$ in the Minkowski space, on which the proper orthochronous Lorentz group

$SO_o(5,1)$ left acts. The augmented stress is a time-like vector moving on hyperboloids inside the cone, which naturally bestows the new model a specific strain-hardening rule as given by Eq. (45).

Numerical tests were conducted by subjecting the new model to different loadings and cyclic loadings. Many important effects and properties regarding the cyclically elastic–plastic behavior were observed. The major cyclic behaviors of materials been able simulated include: smoothing yielding, strain hardening, the Bauschinger effect, cyclic hardening, erasure of memory, mean-stress relaxation, strain ratcheting, as well as out-of-phase hardening. In particular, the existence of equilibrium stress point and limiting surface and the property of erasure-of-memory for the new model have important implications for both the analytical and experimental studies of cyclically stabilized behavior of materials. If further allow the smoothing factor to be a scalar function of λ, it is more good to simulate the saturation of ratcheting strain. Comparisons made with the experimental results of SAE 4340, grade 60 and SS304 steels show that the new model when combining with an appropriate kinematic hardening rule meets certain degree the five requirements that have been proposed by Dafalias (1984) to simulate the cyclic behavior; more significantly, the material parameters used in these simulations are parsimonious.

Acknowledgement

The financial support provided by the National Science Council of Taiwan under the Grant NSC 91-2212-E-019-003 is gratefully acknowledged.

Appendix A

In this section, we prove the following results for the new model.

If $1 < \rho \leqslant 2$, then under the strain path (5) the switch-on time of the new model is given by Eq. (15).

For the strain path given by Eq. (5) and an admissible initial stress $\mathbf{s}(t_{\text{off}})$ specified at time $t = t_{\text{off}}$, dividing Eq. (6) by ρ and by the stressing speed $2G\|\mathbf{c}\|$ we obtain the time elapsed $t_{\text{on}} - t_{\text{off}}$ as shown in Eq. (15).

In view of Fig. 2 and from Eq. (6) we have

$$\mathbf{s}(t_{\text{on}}) \cdot \mathbf{c} = \frac{\|\mathbf{s}(t_{\text{on}})\|\|\mathbf{c}\|}{\sqrt{2}\rho\tau_y^m}\left[\sqrt{2(\tau_y^0)^2 - \|\mathbf{s}(t_{\text{off}})\|^2\sin^2\theta} + (\rho-1)\|\mathbf{s}(t_{\text{off}})\|\cos\theta\right] > 0 \tag{A.1}$$

under the condition $1 < \rho \leqslant 2$. The above inequality asserts that such t_{on} is a switch-on time.

The above results show that for a rectilinear strain path once yielding occurs the new model responds always in the plastic phase up to the termination of the input. The specification of τ_y^m to be a new shear yield strength is equivalent to shorten the original switching-on time given by Eq. (7) to that given by Eq. (15). The smoothing factor ρ cannot be larger than two because it may violate the inequality (A.1) under some initial conditions; for example, $\theta = \pi$, $\|\mathbf{s}(t_{\text{off}})\| = \tau_y^0$ and $\rho = 3$ would make $\mathbf{s}(t_{\text{on}})\cdot\mathbf{c} < 0$.

The modified shear yield strength τ_y^m in the new model satisfies the following inequality:

$$\tau_y^m < \tau_y^0. \tag{A.2}$$

Referring to Fig. 2 we have

$$2(\tau_y^0)^2 = [\|\mathbf{s}(t_{\text{off}})\|\sin(\pi-\theta)]^2 + [\|\Delta\mathbf{s}\| - \|\mathbf{s}(t_{\text{off}})\|\sin(\pi-\theta)]^2. \tag{A.3}$$

Comparing with Eq. (15) for τ_y^m it is obvious that the inequality (A.2) holds.

Appendix B

In this section, we derive a closed-form strain formula for the Prager model under stress control with stress rate constant.

From Eqs. (54) and (56) it follows that

$$\mathbf{e}(t) = \mathbf{e}(t_{\rm on}) + \frac{G + k'}{2Gk'}[\mathbf{s}(t) - \mathbf{s}(t_{\rm on})] + \frac{1}{2k'}[\mathbf{s}_{\rm a}(t_{\rm on}) - \mathbf{s}_{\rm a}(t)], \tag{B.1}$$

where the relative stress is governed by

$$\dot{\mathbf{s}}_{\rm a} + \frac{k'\dot{\lambda}}{\tau_y^0}\mathbf{s}_{\rm a} = \dot{\mathbf{s}} \tag{B.2}$$

in which the plastic multiplier $\dot{\lambda}$ is subjected to

$$\dot{\lambda} = \frac{1}{2k'\tau_y^0}\mathbf{s}_{\rm a}\cdot\dot{\mathbf{s}} > 0 \quad \text{if } \sqrt{2}\tau_y^0 > \|\mathbf{s}_{\rm a}\| \geqslant \sqrt{2}\tau_y^m \text{ and } \mathbf{s}_{\rm a}\cdot\dot{\mathbf{s}} > 0, \tag{B.3}$$

$$\dot{\lambda} = 0 \quad \text{if } \|\mathbf{s}_{\rm a}\| < \sqrt{2}\tau_y^m \text{ or } \mathbf{s}_{\rm a}\cdot\dot{\mathbf{s}} \leqslant 0. \tag{B.4}$$

Upon defining the integrating factor

$$Y^0 := \exp\left(\frac{k'\lambda}{\tau_y^0}\right), \tag{B.5}$$

Eq. (B.2), under the stress path of

$$\mathbf{s}(t) = \mathbf{s}(t_i) + \mathbf{C}(t - t_i) \tag{B.6}$$

with $\mathbf{C}$ a constant second-order deviatoric tensor, becomes

$$\frac{\mathrm{d}}{\mathrm{d}t}(Y^0\mathbf{s}_{\rm a}) = Y^0\mathbf{C}. \tag{B.7}$$

The solution is

$$\mathbf{s}_{\rm a}(t) = \frac{Y^0(t_{\rm on})}{Y^0(t)}\mathbf{s}_{\rm a}(t_{\rm on}) + \int_{t_{\rm on}}^{t}\frac{Y^0(\xi)}{Y^0(t)}\,\mathrm{d}\xi\mathbf{C}. \tag{B.8}$$

From Eqs. (B.5), (B.3), (B.6) and (B.8) we have

$$\dot{Y}^0(t) = \frac{Y^0(t_{\rm on})}{2(\tau_y^0)^2}\mathbf{s}_{\rm a}(t_{\rm on})\cdot\mathbf{C} + \frac{\|\mathbf{C}\|^2}{2(\tau_y^0)^2}\int_{t_{\rm on}}^{t}Y^0(\xi)\,\mathrm{d}\xi. \tag{B.9}$$

A further differential leads to

$$\ddot{Y}^0(t) = \frac{\|\mathbf{C}\|^2}{2(\tau_y^0)^2}Y^0(t), \tag{B.10}$$

whose initial conditions are $Y^0(t_{\rm on})$ and $\dot{Y}^0(t_{\rm on}) = Y^0(t_{\rm on})\mathbf{s}_{\rm a}(t_{\rm on})\cdot\mathbf{C}/(\sqrt{2}\tau_y^0)^2$, and the solution of Eq. (B.10) is

$$Y^0(t) = Y^0(t_{\rm on})[C_1\mathrm{e}^{m(t-t_{\rm on})} + C_2\mathrm{e}^{-m(t-t_{\rm on})}], \tag{B.11}$$

where

$$m := \frac{\|\mathbf{C}\|}{\sqrt{2}\tau_y^0}, \quad C_1 := \frac{1}{2}\left[1 + \frac{\mathbf{s}_a(t_{on})\cdot\mathbf{C}}{m(\tau_y^0)^2}\right], \quad C_2 := \frac{1}{2}\left[1 - \frac{\mathbf{s}_a(t_{on})\cdot\mathbf{C}}{m(\tau_y^0)^2}\right]. \tag{B.12}$$

Substituting Eq. (B.11) into Eq. (B.8) and integrating give a closed-form stress formula:

$$\mathbf{s}_a(t) = \frac{\mathbf{s}_a(t_{on}) + \{C_1[e^{m(t-t_{on})} - 1] + C_2[1 - e^{-m(t-t_{on})}]\}\bar{\mathbf{C}}}{C_1 e^{m(t-t_{on})} + C_2 e^{-m(t-t_{on})}}, \tag{B.13}$$

where

$$\bar{\mathbf{C}} := \frac{\sqrt{2}\tau_y^0\mathbf{C}}{\|\mathbf{C}\|}. \tag{B.14}$$

Inserting Eq. (B.13) into Eq. (B.1) we can calculate **e**.

References

Abdel-Karim, M., Ohno, N., 2000. Kinematic hardening model suitable for ratchetting with steady-state. Int. J. Plasticity 16, 225–240.

Bari, S., Hassan, T., 2000. Anatomy of coupled constitutive models for ratcheting simulation. Int. J. Plasticity 16, 381–409.

Bari, S., Hassan, T., 2001. Kinematic hardening rules in uncoupled modeling for multiaxial ratcheting simulation. Int. J. Plasticity 17, 885–905.

Bari, S., Hassan, T., 2002. An advancement in cyclic plasticity modeling for multiaxial ratcheting simulation. Int. J. Plasticity 18, 873–894.

Chaboche, J.L., 1986. Time-independent constitutive theories for cyclic plasticity. Int. J. Plasticity 2, 149–188.

Chaboche, J.L., 1991. On some modifications of kinematic hardening to improve the description of ratchetting effects. Int. J. Plasticity 7, 661–678.

Chaboche, J.L., 1994. Modeling of ratchetting: evaluation of various approaches. Eur. J. Mech. A/Solids 13, 501–518.

Chaboche, J.L., Jung, O., 1998. Application of kinematic hardening viscoplasticity model with thresholds to the residual stress relaxation. Int. J. Plasticity 13, 785–807.

Chiang, D.Y., 1997. A phenomenological model for cyclic plasticity. J. Engrg. Mat. Tech., ASME 119, 7–11.

Chiang, D.Y., 1998. The concept of plastic equilibrium points and its applications in cyclic plasticity. Int. J. Plasticity 14, 933–943.

Chiang, D.Y., Beck, J.L., 1994. A new class of distributed-element models for cyclic plasticity—I. Theory and application, II. Important properties of material behavior. Int. J. Solids Struct. 31, 469–496.

Chiang, D.Y., Su, K.H., Liao, C.H., 2002. A study on subsequent yield surface based on the distributed-element model. Int. J. Plasticity 18, 51–70.

Corona, E., Hassan, T., Kyriakides, S., 1996. On the performance of kinematic hardening rules in predicting a class of biaxial ratcheting histories. Int. J. Plasticity 12, 117–145.

Dafalias, Y.F., 1984. Modelling cyclic plasticity: simplicity versus sophistication. In: Desai, C.S., Gallagher, R.H. (Eds.), Mechanics of Engineering Materials. John Wiley, New York, pp. 153–178.

Dafalias, Y.F., Popov, E.P., 1975. A model of nonlinearly hardening materials for complex loading. Acta Mech. 21, 173–192.

Dafalias, Y.F., Popov, E.P., 1976. Plastic internal variables formalism of cyclic plasticity. J. Appl. Mech., ASME 98, 645–651.

Delobelle, P., Robinet, P., Bocher, L., 1995. Experimental study and phenomenological modelization of ratchet under uniaxial and biaxial loading on an austenitic stainless steel. Int. J. Plasticity 11, 295–330.

Drucker, D.C., 1959. A definition of stable inelastic material. J. Appl. Mech., ASME 26, 101–106.

Drucker, D.C., 1988. Conventional and unconventional plastic response and representation. Appl. Mech. Rev., ASME 41, 151–167.

Hale, J.K., 1969. Ordinary Differential Equations. Wiley, New York.

Hashiguchi, K., 1988. A mathematical modification of two surface model formulation in plasticity. Int. J. Solids Struct. 24, 987–1001.

Hashiguchi, K., 1989. Subloading surface model in unconventioal plasticity. Int. J. Solids Struct. 25, 917–945.

Hashiguchi, K., 1993. Mechanical requirements and structures of cyclic plasticity models. Int. J. Plasticity 9, 721–748.

Hassan, T., Kyriakides, S., 1992. Ratcheting in cyclic plasticity, Part I: uniaxial behavior, Part II: multiaxial behavior. Int. J. Plasticity 8, 91–146.

Haupt, P., Kamlah, M., 1995. Representation of cyclic hardening and softening properties using continuous variables. Int. J. Plasticity 11, 267–291.

Hong, H.-K., Liu, C.-S., 1997. Prandtl–Reuss elastoplasticity: on–off switch and superposition formulae. Int. J. Solids Struct. 34, 4281–4304.

Hong, H.-K., Liu, C.-S., 1998. On behavior of perfect elastoplasticity under rectilinear paths. Int. J. Solids Struct. 35, 3539–3571.

Hong, H.-K., Liu, C.-S., 1999. Lorentz group $SO_o(5,1)$ for perfect elastoplasticity with large deformation and a consistency numerical scheme. Int. J. Non-Linear Mech. 34, 1113–1130.

Hong, H.-K., Liu, C.-S., 2000. Internal symmetry in the constitutive model of perfect elastoplasticity. Int. J. Non-Linear Mech. 35, 447–466.

Iwan, W.D., 1966. A distributed element model for hysteresis and its steady-state dynamic response. J. Appl. Mech., ASME 33, 893–900.

Iwan, W.D., 1967. On a class of models for the yielding behavior of continuous and composite systems. J. Appl. Mech., ASME 34, 612–617.

Jiang, Y., Sehitoglu, H., 1994a. Cyclic ratchetting of 1070 steel under multiaxial stress states. Int. J. Plasticity 10, 579–608.

Jiang, Y., Sehitoglu, H., 1994b. Multiaxial cyclic ratchetting under multiple step loading. Int. J. Plasticity 10, 849–870.

Jiang, Y., Sehitoglu, H., 1996. Comments on the Mroz multiple surface type plasticity models. Int. J. Solids Struct. 33, 1053–1068.

Kang, G., Gao, Q., 2002. Uniaxial and non-proportionally multiaxial ratcheting of U71Mn rail steel: experiments and simulations. Mech. Mater. 34, 809–820.

Kang, G., Gao, Q., Yang, X., 2002a. Uniaxial cyclic ratcheting and plastic flow properties of SS304 stainless steel at room and elevated temperatures. Mech. Mater. 34, 145–159.

Kang, G., Gao, Q., Yang, X., 2002b. A visco-plastic constitutive model incorporated with cyclic hardening for uniaxial/multiaxial ratcheting of SS304 stainless steel at room temperature. Mech. Mater. 34, 521–531.

Klisiński, M., Mróz, Z., 1988. Description of inelastic deformation and degradation of concrete. Int. J. Solids Struct. 24, 391–416.

Krieg, R.D., 1975. A practical two surface plasticity theory. J. Appl. Mech., ASME 42, 641–646.

Lamba, H.S., Sidebottom, O.M., 1978. Cyclic plasticity for nonproportional paths: part 1—cyclic hardening, erasure of memory, and subsequent strain hardening experiments, part 2—comparison with predictions of three incremental plasticity models. J. Engrg. Mat. Tech., ASME 100, 96–111.

Liu, C.-S., 2000. A Jordan algebra and dynamic system with associator as vector field. Int. J. Non-Linear Mech. 35, 421–429.

Liu, C.-S., 2001. Cone of non-linear dynamical system and group preserving schemes. Int. J. Non-Linear Mech. 36, 1047–1068.

Liu, C.-S., 2003. Smoothing elastoplastic stress–strain curves obtained by a critical modification of conventional models. Int. J. Solids Struct. 40, 2121–2145.

Liu, C.-S., 2004. A consistent numerical scheme for the von Mises mixed-hardening constitutive equations. Int. J. Plasticity 20, 663–704.

Liu, C.-S., Chang, C.-W., 2005. Non-canonical Minkowski and pseudo-Riemann frames of plasticity models with anisotropic quadratic yield criteria. Int. J. Solids Struct. 42, 2851–2882.

Liu, C.-S., Hong, H.-K., 2000. The contraction ratios of perfect elastoplasticity under biaxial controls. Eur. J. Mech. A/Solids 19, 827–848.

Masing, G., 1926. Eigenspannungen und verfestigung beim messing (Self stretching and hardening for brass). In: Proceeding of 2nd International Congress for Applied Mechanics, Zurich, Switzerland, pp. 332–335.

McDowell, D.L., 1995. Stress state dependence of cyclic ratchetting behavior of two rail steels. Int. J. Plasticity 11, 397–421.

Mizuno, M., Mima, Y., Abdel-Karim, M., Ohno, N., 2000. Uniaxial ratchetting of 316FR steel at room temperature—Part I: experiments. J. Engrg. Mater. Tech., ASME 122, 29–34.

Mróz, Z., 1967. On the description of anisotropic workhardening. J. Mech. Phys. Solids 15, 163–175.

Mróz, Z., Norris, V.A., Zienkiewicz, O.C., 1979. Application of an anisotropic hardening model in the analysis of elasto-plastic deformation of soils. Geotechnique 29, 1–34.

Mróz, Z., Norris, V.A., Zienkiewicz, O.C., 1981. An anisotropic, critical state model for soils subjected to cyclic loading. Geotechnique 31, 451–469.

Ohno, N., Abdel-Karim, M., 2000. Uniaxial ratchetting of 316FR steel at room temperature—Part II: constitutive modeling and simulation. J. Engrg. Mater. Tech., ASME 122, 35–41.

Ohno, N., Wang, J.-D., 1993. Kinematic hardening rules with critical state of dynamic recovery, Part I: formulation and basic features for ratchetting behavior, Part II: application to experiments of ratchetting behavior. Int. J. Plasticity 9, 375–403.

Ohno, N., Wang, J.-D., 1994. Kinematic hardening rules for simulation of ratchetting behavior. Eur. J. Mech. A/Solids 13, 519–531.

Ottosen, N.S., Ristinmaa, M., 1996. Corners in plasticity—Koiter's theory revisited. Int. J. Solids Struct. 33, 3697–3721.

Portier, L., Calloch, S., Marquis, D., Geyer, P., 2000. Ratchetting under tension–torsion loadings: experiments and modelling. Int. J. Plasticity 16, 303–335.

Prager, W., 1956. A new method of analyzing stresses and strains in work-hardening plastic solids. J. Appl. Mech., ASME 23, 493–496.

Prandtl, L., 1924. Spannungsverteilung in plastischen kœrpern. In: Proceedings of the 1st International Congress on Applied Mechanics, Delft, pp. 43–54.

Ramrakhyani, D.S., Lesieutre, G.A., Smith, E.C., 2004. Modeling of elastomeric materials using nonlinear fractional derivative and continuously yielding friction elements. Int. J. Solids Struct. 41, 3929–3948.

Reuss, E., 1930. Beruecksichtigung der elastischen formaenderungen in der plastizitaetstheorie. Zeits Angew. Math. Mech. (ZAMM) 10, 266–274.

Ristinmaa, M., 1995. Cyclic plasticity model using one yield surface only. Int. J. Plasticity 11, 163–181.

Shiao, Y.-P., 2000. A study on multiaxial cyclic loading and anisotropic plasticity of structural metals. Ph.D. Dissertation, Department of Civil Engineering, National Taiwan University, Taipei.

Taheri, S., Lorentz, E., 1999. An elastic–plastic constitutive law for the description of uniaxial and multiaxial ratchetting. Int. J. Plasticity 15, 1159–1180.

Tseng, N.T., Lee, G.C., 1983. Simple plasticity model of two-surface type. J. Engrg. Mech. ASCE 109, 795–810.

Voyiadjis, G.Z., Sivakumar, S.M., 1991. A robust kinematic hardening rule with ratchetting effects: Part I. Theoretical formulation. Acta Mech. 90, 105–123.

Voyiadjis, G.Z., Sivakumar, S.M., 1994. A robust kinematic hardening rule with ratchetting effects: Part II. Application to nonproportional loading cases. Acta Mech. 107, 117–136.

Whiteman, I.R., 1959. A mathematical model depicting the stress–strain diagram and the hysteresis loop. J. Appl. Mech., ASME 26, 95–100.

Xia, Z., Ellyin, F., 1997. A constitutive model with capability to simulate complex multiaxial ratcheting behaviour of materials. Int. J. Plasticity 13, 127–142.